AD-A172 871 SPECTROSCOPIC AND LASER CHARACTERIZATION EMERALD(U) 1/1
ALLIED-SIGNAL INC MORRISTOWN NJ ELECTRONIC MATERIALS
AND DEVICES LAB S T LAI ET AL. AUG 86 ARO-20240.6-PH
UNCLASSIFIED DAAG29-83-C-0015 F/G 20/6 NL

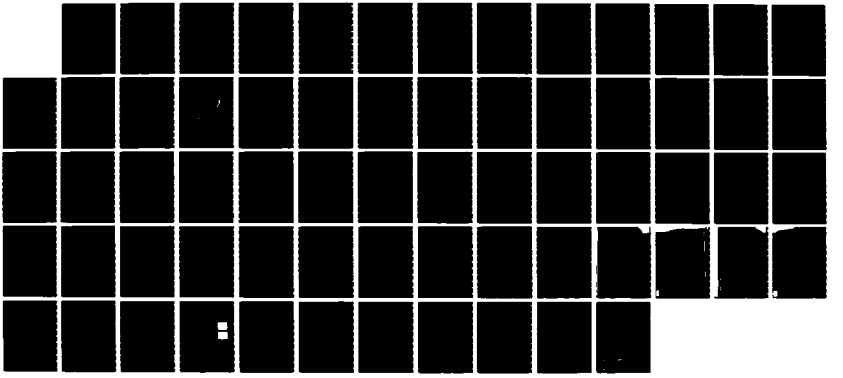

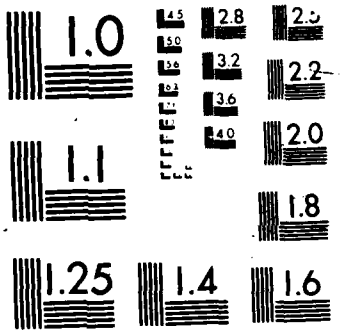
1.0
1.1
1.25
1.4
1.6
2.8
3.2
3.6
4.0
2.2
2.0
1.8

FINAL TECHNICAL REPORT

SPECTROSCOPIC AND LASER CHARACTERIZATION OF EMERALD

Electronic Materials and Devices Laboratory
CORPORATE TECHNOLOGY

Contract DAAG29-83-C-0015

Submitted To:
U.S. Army Research Office
P.O. Box 1211
Research Triangle Park, NC 27709-2211

August, 1986

ALLIED

Spectroscopic and Laser Characterization of Emerald

Final Report

by

Shui T. Lai and Bruce H.T. Chai

August 8, 1986

U.S. Army Research Office

Grant Number: DAAG 29-83-C-0015

Allied-Signal, Inc.

Morristown, New Jersey

UNCLASSIFIED
SECURITY CLASSIFICATION OF THIS PAGE (When Data Entered)

MASTER COPY - FOR REPRODUCTION PURPOSES

REPORT DOCUMENTATION PAGE		READ INSTRUCTIONS BEFORE COMPLETING FORM
1. REPORT NUMBER ARO 20240.6-PH	2. GOVT ACCESSION NO. N/A	3. RECIPIENT'S CATALOG NUMBER N/A
4. TITLE (and Subtitle) Spectroscopic and laser characterization of emerald.		5. TYPE OF REPORT & PERIOD COVERED Final report, April, 1983-April, 1986 6. PERFORMING ORG. REPORT NUMBER
7. AUTHOR(s) Lai, S.T. and Chai, B.H.T.		8. CONTRACT OR GRANT NUMBER(s) DAAG-29-83-C-0015
9. PERFORMING ORGANIZATION NAME AND ADDRESS Allied-Signal, Inc. P.O. Box 1021R Morristown, NJ 07960		10. PROGRAM ELEMENT, PROJECT, TASK AREA & WORK UNIT NUMBERS
11. CONTROLLING OFFICE NAME AND ADDRESS U. S. Army Research Office Post Office Box 12211 Research Triangle Park, NC 27709		12. REPORT DATE August, 1986 13. NUMBER OF PAGES 58
14. MONITORING AGENCY NAME & ADDRESS(if different from Controlling Office)		15. SECURITY CLASS. (of this report) Unclassified 15a. DECLASSIFICATION/DOWNGRADING SCHEDULE

16. DISTRIBUTION STATEMENT (of this Report)

Approved for public release; distribution unlimited.

17. DISTRIBUTION STATEMENT (of the abstract entered in Block 20, if different from Report)

NA

18. SUPPLEMENTARY NOTES

The view, opinions, and/or findings contained in this report are those of the author(s) and should not be construed as an official Department of the Army position, policy, or decision, unless so designated by other documentation.

19. KEY WORDS (Continue on reverse side if necessary and identify by block number)

Emerald laser characteristics and spectroscopy, laser efficiency and laser measurements. Excited state absorption. Single-pass gain measurements. Emerald crystal growth.

20. ABSTRACT (Continue on reverse side if necessary and identify by block number)

The spectroscopic characteristics and laser properties of emerald were investigated. The laser measurements showed that the emerald laser tuning range was 720-842 nm and exhibited a high gain and high efficiency in the 760-790 nm range. Under a crystal growth development program, the laser loss has been reduced from 11%/cm to 0.4%/cm. The limiting factor in the laser efficiency is the excited state absorption (ESA). The ESA was measured by two methods: A laser-pumped single-pass gain method, which is generally applicable to all

DD FORM 1 JAN 73 1473 EDITION OF 1 NOV 65 IS OBSOLETE

UNCLASSIFIED
SECURITY CLASSIFICATION OF THIS PAGE (When Data Entered)

tunable laser materials, and a laser-pumped laser method. A 76% laser quantum yield was obtained in high optical quality emerald. The maximum yield is estimated to be 83%, based on the ESA measurements.

A-1

Table of Contents

List of Appendixes

List of Tables

List of Figures

Forward

The discovery of alexandrite laser and the subsequent demonstration of its high efficiency and high power operation opened up the field of room temperature tunable lasers. The list of newly discovered lasers is quite extensive, but only a small group of the new lasers can operate at room temperature. Still fewer can be flashlamp-pumped and operate with stability and reasonable efficiency. Results of the spectroscopic measurements and laser testings of this project indicated that emerald laser has high efficiency, comparable to that of alexandrite and high gain, about three times that of alexandrite. No color center formation was observed under flashlamp-pumped operation. At the start of this program, only gem quality emerald was available. The efficiency of the early flashlamp-pumped laser result was quite low. A parallel program on emerald crystal growth was implemented along with the laser characterization. The optical quality of emerald has been steadily improved from gem quality to laser quality. The laser scattering loss has been reduced from 11%/cm to 0.4%/cm. Emerald had a laser tuning range of 720-842 nm, and high gain in the 750-790 nm region. It posted competition to alexandrite, and had a better performance than Cr doped GSGG or GSAG. To date, emerald is the room temperature Cr tunable laser with the highest gain, and operates with high efficiency.

1. Program Overview

The scope of this project is to characterize the spectroscopic and laser properties of emerald. Our focus was on the physical parameters which were electronic in nature and were intrinsic to the Cr^{3+} in a beryl crystal structure. These parameters were essential in the modeling of laser performance, and in determining the limits within which the laser can operate. Laser efficiency was the principal factor in the evaluation of emerald lasers. The overall efficiency was considered in three parts: (1) the pump efficiency, (2) the fluorescence efficiency, and (3) the lasing efficiency. The Cr^{3+} absorption bands in emerald had excellent coverage of the visible spectrum. Good pump efficiency could be attained with either a blackbody-like continuum source, such as a flashlamp or narrow band laser lines. In a finely tuned laser-pumped laser, emerald has been shown to have a 64% output slope efficiency, corresponding to a laser quantum yield of 76%. These numbers indicated good optical quality and high fluorescence quantum yield in emerald. The excited state absorption (ESA) was a determining material parameter which limited the tuning range and the laser efficiency in emerald. The Cr^{3+} transition between the laser level $^4T_2$ to the ground state $^4A_2$ is mostly phonon-assisted, resulting in the broad fluorescence band and its tunability. However the phonon-coupling also makes the transition from the lowest excited state, the ^2E and $^4T_2$ to the higher electronic levels allowed. This upward transition competes for the pump photons and the laser photons. This photon drain causes laser loss. In the case of high power laser operation, the ESA was a more important consideration than the lesser optical quality of the laser medium. The ESA is intrinsic to the laser material and cannot be improved as does the optical quality of the material or the design of laser oscillator. The excited state absorption cross sections were measured by a single-pass gain method. We modified a flashlamp-pumped single-pass setup to

increase accuracy. A cw pump source and a cw probe beam from a dye laser were used to enhance the signal to noise ratio. A new technique was also developed to deduce the ESA from laser measurements. The ratio of the ESA cross section to the emission cross section at the lasing wavelength was measured through the slope of output power vs. input curve. The lowest measured ESA was at 768 nm with a ESA to emission cross section ratio of 20% from laser measurement. It was slightly higher than the 14% measured at 756 nm in alexandrite.

In prototype laser testing, we used a finely tuned high efficiency laser-pumped cavity for the evaluation of emerald laser performance. The object was to achieve as closely as possible a 100% accountability of photon absorbed in the gain medium. Earlier measurements showed an 85% overall laser quantum yield in a similar cavity for alexandrite[1]. In controlled measurements, emerald laser performance was evaluated based on its output power slope efficiency and threshold pump power and the maximum output power before it deviated from a linear slope. The optical quality of emerald was monitored by measuring the scattering loss in the material. This information was used to improve the crystal growth processes. Emerald laser had a tuning range from 720 nm to 842 nm. The highest measured output slope was 64%. The maximum laser quantum yield in emerald based on the emission cross sections and the ESA was estimated to be 83%.

The emerald available at the start of this project was gem quality crystals. Large amount of impurities such as V and Fe were incorporated in the crystal to quench the fluorescence to enhance the "emerald green" color. A parallel program to develop laser quality emerald crystals was implemented. Poor fluorescence efficiency, cracks, optical inhomogeneity, and index of refraction

gradient were among the problems of earlier crystals. Few choices are available for the emerald growth. Czochralski method could not be used due to the fact that emerald did not form congruent melt. Hydrothermal growth was chosen for high optical quality and its reasonable growth cycle. The emerald growth program proceeded in two fronts. An in-house emerald growth facility was constructed to develop large crystal growth. Growth chambers were designed for sufficiently large emeralds for laser applications in either rod or slab forms. For near-term supply, we collaborated with the Vacuum Ventures, Inc., a commercial emerald gem grower. To maintain a desirable solubility level in the nutrient, the growth chamber was kept at a pressure of 12,000 psi at 600°C. In addition to the damage that might have been caused by explosion, the Be content in the starting materials also posted serious health concerns. The in-house growth chamber had gone through a series of modifications and some major redesign. We have completed four growth runs successfully. The growth parameters were still to be optimized. We proceeded with great caution and we did not have any accidents so far. The improvements on the Vacuum Ventures emerald has been very steady. The index of refraction gradient which caused beam breakup in the earlier emeralds was largely eliminated. The scattering loss has also been reduced from 11%/cm in the early crystals to 0.4%/cm from the latest runs. However the Vacuum Ventures emeralds were limited in size and the high optical quality portion of the growth was at about a 50% point of the entire growth volume. From what we have developed so far, it is clear that high laser quality emerald can be grown by hydrothermal technique. More developments are underway to scale up the crystal size.

2. Laser-relevent Spectroscopic Parameters of Emerald

Laser-relevent spectroscopic parameters can in general be categorized according to three aspects of laser operation: (1) absorption of the pump light, (2) followed by the fluorescence and stimulated emission and (3) laser action if there is a sufficient gain in the laser medium. Each aspect is considered in the following.

2.1 Absorption

The energy levels of the optially active ions Cr^{3+} in emerald were well studied. Two broad absorption bands, $^4T_2$ and $^4T_1$ in emerald covered significant portions of the visible spectrum (Appendix 1). The absorption cross sections were calculated based on the Cr concentration measured by a neutron activation method[2]. The peak absorption cross sections of the $^4T_2$ band polarized along the c-axis (pi) and polarized perpendicular to the c-axis (sigma) are 8.26 x 10^{-20} cm^2 at 650 nm and 0.56 x 10^{-20} at 600 nm, respectively. They are about half of those in ruby[3]. Emerald has the capacity of incorporating high Cr concentration without compromising the crystal quality. No evidence of Cr pair structures or fluorescence quenching were observed in emerald with Cr concentrations up to 3 at%. The optical density was 1.4 at 650 nm in a 3 mm thick emerald with a Cr concentration of 2.2 at% (Fig. 3 in Appendix 1). The high attainable optical density in emerald has the advantage of attaining high excited state density in a small volume, and hence a lower laser threshold. This is especially important for cw laser operation, and for laser configurations using close-coupled diode-pumping.

The relative pump efficiency in emerald was studied with excitation spectra. By monitoring the fluorescence intensity, a narrow band excitation source was

scanned spectrally through the visible spectrum. The polarized excitation spectra, both in the pi-polarization and in the sigma-polarization, had almost perfect match for the $^4T_1$ band and a better than 90% match for the $^4T_2$ band, indicating a nearly unity relative fluorescence efficiency throughout the Cr absorption in the visible spectrum.

2.2 Fluorescence

The site symmetry at the Cr ion plays an important role on the oscillator strength of the laser transition. In emerald, the six-fold coordinated oxygen bonds at the Cr ion were distorted from a perfect octahedron. The largest shift of bond angle for an O-Cr-O coordination reached 14°[4]. The low site symmetry accounts for the relatively short transition time of 33 μs, between the $^4T_2$ level and the ground state $^4A_2$[5]. At room temperature, the emerald fluorescence lifetime was 60 μs. We believe that the spatial separation of the Al octahedra in the beryl crystal structure accounted for the lack of concentration quenching in emerald. There is only a single type of Cr site in emerald, unlike some Cr doped laser material, such as $SrAlF_5$[6], in which some of the inequivalent sites are nonradiactive and severely limits its laser efficiency. The fluorescence decay was a single exponential. No lifetime variation was measured across the fluorescence bandwidth. Direct measurement of the radiative efficiency was not made. But the low laser threshold in the laser pumped emerald lasers indicated that its efficiency was comparable to that of alexandrite, the quantum efficiency of which was about 95%[7]. At elevated temperatures, the fluorescence lifetime decreased according to a Boltzman distribution of the excited state populations between the ^2E and $^4T_2$ levels. Above 250°C, the lifetime dropped at a much faster rate, due to multiphonon-assisted relaxation from the $^4T_2$ to

the ground state $^4A_2$. We speculated from the fluorescence versus lifetime curve (Appendix 1) that the fluorescence efficiency remained high to 200C. The stimulated emission cross sections σ_e were calculated using the fluorescence lifetime and an average value of 1.58 for index of refraction and is shown in Fig. 1. The peak of the emission cross section increased from 3.1 x 10^{-20} cm^2 at 28C to 3.9 x 10^{-20} cm^2 at 200C. It shifted from 750 nm at 28C towards slightly longer wavelengths with increasing temperatures. For high peak power laser operation, the saturation fluence E_{sat}, the photon flux required to extract energy from the laser medium by depleting the population to its e^{-1} fold of its initial value in a single pass, was estimated. At room temperature, emerald has a E_{sat} of 8.4 Joule/cm^2, which is very low among tunable vibronic lasers ($Ti^{3+}:Al_2O_3$ has an order of magnitude smaller E_{sat}, but its 3 μs fluorescence lifetime posts difficulty and limitation on the pump source). The emerald E_{sat} is comparable to those of the Nd:glasses presently used ultra-high peak power lasers.

2.3 Laser Action

The laser losses can be classified in two categories: (1) the intrinsic losses associated with the Cr^{3+} electronic transitions, and (2) the extrinsic losses due to the less than ideal optical quality of the material, impurity absorption loss, and thermally-induced lensing and birefringence. In the gain medium, several active processes are competing for the laser photon: the stimulated emission which provides for the gain in laser action, the absorption from the metastable levels $^4T_2$ and ^2E to a higher excited state, and the absorption from the ground state to the metastable state. The latter two processes were the principal sources of the intrinsic laser losses. At room temperature, ground state absorption in emerald extended well below the ^2E - $^4A_2$ energy gap (14500 cm^{-1}), and was only negligible below 13600 cm^{-1}. The lower bound of the

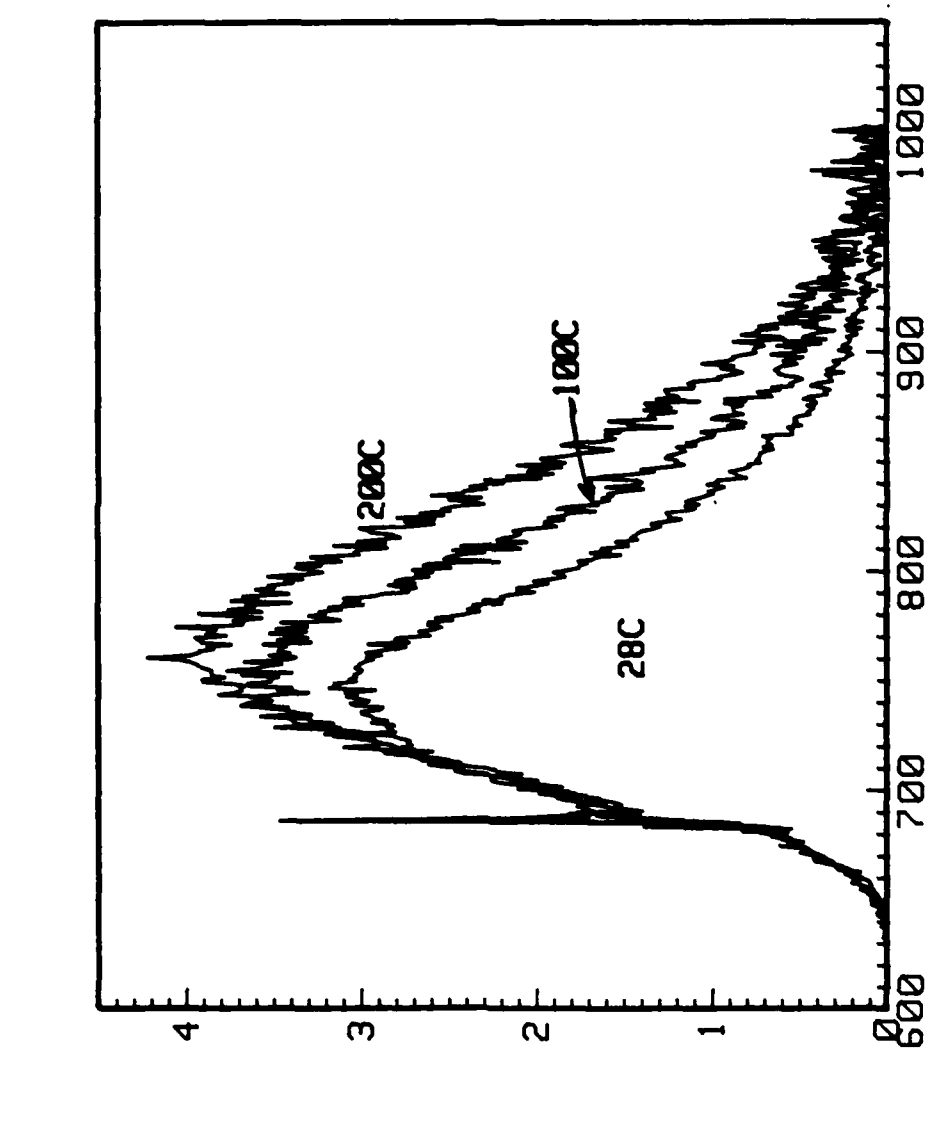

Figure 1. The stimulated emission cross sections of emerald at different temperatures. The cross sections are in the units of 10^{-20} cm^2.

laser tuning range (720 nm) was limited by the ground state absorption process. The excited state absorption process (σ_{2a}) competes with the emission process (σ_e) at all laser wavelengths. Even in an ideal laser host with negligible extrinsic losses, the laser efficiency would still be limited to $\sigma_e/(\sigma_e + \sigma_{2a})$. The extrinsic losses further lowered the laser efficiency. The extent of the deviation from the ideal efficiency (zero extrinsic loss) gives an overall evaluation of the laser performance as limited by the extrinsic losses. In emerald, the efficiency limit was estimated to be 83%, at 768 nm, and the measured laser quantum yield was 76% in our good quality emerald. The deviation was less than 10% of the efficiency limit. Considering the extrinsic losses alone, the material can deliver over 90% efficiency in comparison to a 83% limit due to the Cr^{3+} electronic excited state absorption process. These results indicates the high optical quality in crystal and the high overall laser performance attainable in emerald.

3. Excited State Absorption Cross Section Measured by Single-pass Gain Method

The 3d electrons of the Cr^{3+}, being in the outermost shell, interact strongly with its host lattice. The transition between the $^4T_2$ and $^4A_2$ is mostly phonon-assisted. The no-phonon oscillator strength is negligible compared to its vibronic side band. Unlike rare earth ions, there is no strictly forbidden transition at any photon energy above the ^2E - $^4A_2$ gap in emerald. While this property was recognized as an advantage over the rare earth ions in its absorption efficiency when broadband pump sources were used, it also provided a channel for energy drain. Absorption of the laser photon at the metastable states $^4T_2$ and ^2E competed with the stimulated laser emission pro-

cess. As crystal quality continued to improve by better growth techniques, the extrinsic material losses became negligible, the excited state absorption (ESA) process became the important factor controlling the laser efficiency. With the exception of the d^1 and possibly d^9 electronic configurations, ESA exists in all transition metal ion lasers. Measurement techniques were developed for this important laser parameter.

The excited state absorption can be divided into two spectral regions of interest: (1) the laser wavelength region where the stimulated emission is non-zero, and (2) the pump source wavelength region. For emerald, the pump photons with energy below the ^2E level do not contribute to the laser population and only cause heat load by cycling the excited state ions between ^2E and the upper electronic levels. At the pump wavelengths where the emission cross section is negligible, the absorption cross section can be determined relatively simply if the excited state density is known. With an incoherent, broadband pump source, the determination of the excited state density was not obvious. Fairbank, et.al.[8] developed a technique for Cr^{3+} laser materials which had sharp R-lines absorption, typical of those in high crystal field hosts where the ^2E was sufficiently below the $^4T_2$ levels. They monitored the change in the absorbance of the sharp line as an indicator of the excited state population. This method worked well with ruby and emerald[8], and it was later used in alexandrite[9]. However, for Cr doped GSGG, $KZnF_3$, $ScBO_3$ or $SrAlF_5$, the method was not applicable due to the absence of prominent sharp feature in the absorption spectra.

A generally applicable method using a laser as the pump source was developed. There are several advantages in using laser pumping. The amount of pump photons absorbed in the laser medium could be accurately measured. The steady

state density could be calculated from the measured pump beam waist in the sample. The physical size of required laser sample was usually small, the minimum size being the dimensions of the laser beam cross section area and the depth which was typically less than 1 cm, depending on the optical density. In a flashlamp-pumped cavity, the material was usually in the form of a rod a couple of inches in length. The time and efforts required to produce good quality material large enough for a laser rod could be substantial compared to that for a smaller piece usable for the laser-pumped method. In the search for new laser materials, an earlier determination of the laser limitations could help to redirect resources to more fruitful paths.

Details of the experimental setup were reported earlier and is included in Appendix 2. The TEM_{oo} laser mode was maintained in both the pump and the probe beam. The gain profile in the emerald was therefore also a Gaussian. We took into account a Gaussian probe beam in a Gaussian gain profile by integrating the spatial distribution of the gain. An approximated expression which has a cutoff above the second order term was given in Equation (3) in Appendix 2. The exact solution in close form was obtained later and is included here:

$$P_p/P_u = \frac{\exp(\gamma) - 1}{\gamma} \qquad (1)$$

where P_p and P_u are the measured probe beam intensities with the pump beam on and the pump beam off, respectively, and γ is given by

$$\gamma = \frac{2 P_{abs} \tau}{h\nu_{pump} \pi \omega_{pump}^2} \xi (\sigma_e + \sigma_a - \sigma_{2a}) \qquad (2)$$

where τ is the fluorescence lifetime, P_{abs} is the absorbed pump power, $h\nu_{pump}$ is the pump photon energy, $\pi\omega_{pump}^2$ gives approximately the pump beam cross sectional area. σ_a and σ_{2a} are the ground state and the excited state absorption

cross sections at the probe wavelength, and ξ is the factor which accounts for efficiency of the pump, due to the small amount of the energy drain by the ESA of the pump photon.

The factor ξ can be measured directly or calculated using an expression which included the absorption coefficients of the ground state and the excited state Cr at the pump wavelength. The ξ could also be measured from the sub-linear behavior of the single-pass gain as a function of the pump power. With 2.2 watts of absorbed pump power at 647.1 nm. and a pump beam waist (radius) of 155 μm, ξ was 0.97. One important feature in equation (1) is that the Cr concentration is absent in the expression. With the calculated σ_e and σ_a, the ESA cross section σ_{2a} could be obtained from equation (1) by measuring the single-pass gain (SPG). One difficulty in the SPG measurement was the probe beam movement at the optical detector due to the thermal lensing. Because the SPG was typically 3~5% depending on how tight the pump beam focused, small variation in sensitivity over the detector surface could cause significant spurious signals. The beam movement was largely eliminated by collimating optics so that the beam position became insensitive to the beam divergence.

The single-pass gain as a function of the probe beam wavelength is shown in Figure 2. An average was taken over several data sets. The rapid rise of of the SPG below 725 nm was due to the fluorescence interference at a weak probe beam intensity. By extrapolation, the gain curve indicated a net positive gain beyond 840 nm. With equation (1), the σ_{2a} was calculated and is shown in Figure 3. The σ_{2a} remained relatively constant throughout

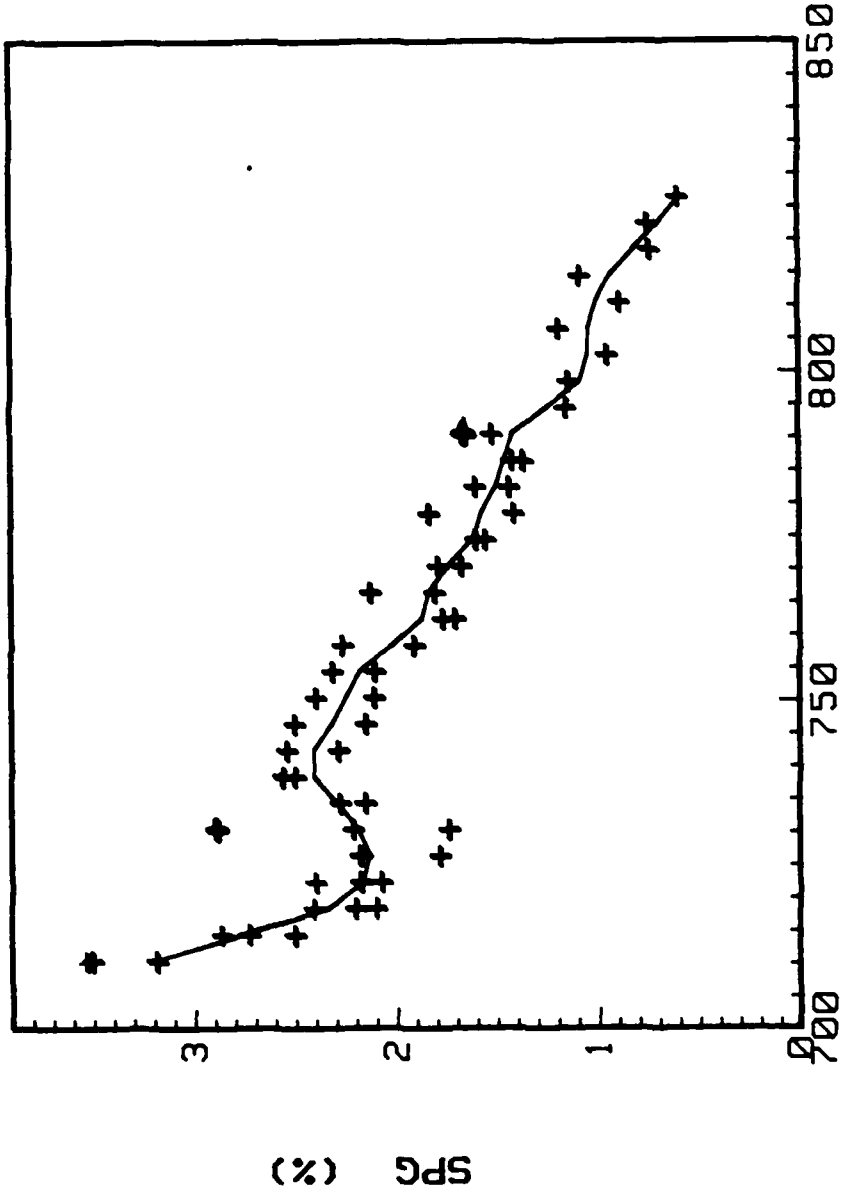

Figure 2. The single-pass gain (SPG) values of the probe beam as a function of wavelength. The E-field of probe beam was parallel to the c-axis.

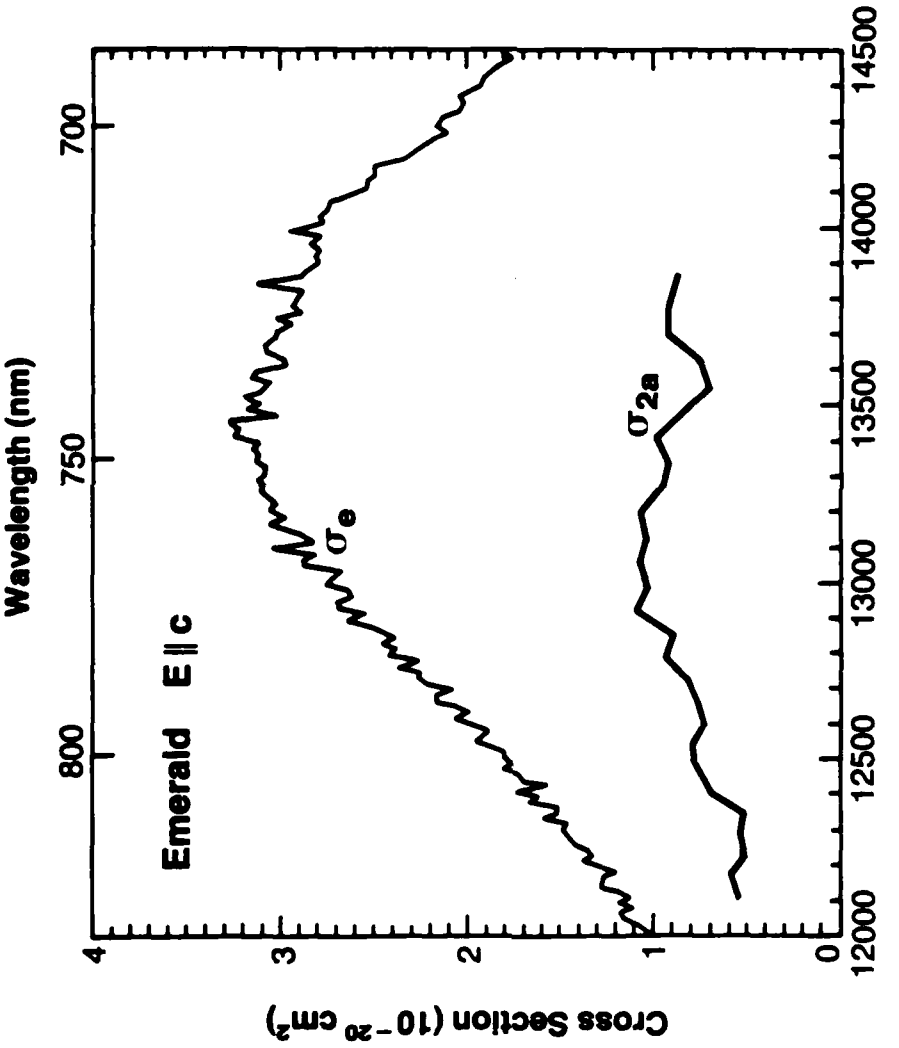

Figure 3. The calculated excited state absorption cross sections σ2a from SPG measurements. The σ_e spectrum is included for comparison. Both spectra are π-polarized.

the probe wavelength range. The variation in the SPG was a reflection of the stimulated emission cross section. We also noted from Figure 3 that the (σ_e - σ_{2a}) value remained high near 720 nm. However the emerald laser action was cutoff below 720 nm in our laser measurement. The $^4T_2$ absorption tail extended well below the ^2E level at room temperature, the lower end of the laser tuning range was understood to be limited by the ground state absorption process. At higher temperatures, we expect the lower limit to be further pushed toward longer wavelengths. A root-mean-square (RMS) error analysis was performed to give an estimate of the accuracy of the σ_{2a}'s. The reuslts are shown in Table I. The parameter values used in the calculation are given in the second column. The estimated standard deviation errors are listed in column three. The RMS fluctuations of the σ_{2a} as a result of the SD of each parameter are listed in the last column. The total σ_{2a} fluctuation is also given in the last row of the table.

TABLE I. Fluctuation of the calculated σ_{2a} due to standard deviations (SD) of the measured parameters.

		SD	RMS variation of σ_{2a} (10^{-22} cm^2)
Lifetime (μsec)	60	1•2	3•8
Power absorbed (watt)	2•2	0•1	9•5
SPG	2%	0•15%	14
Pump beam waist (μm)	155	6 (23)	14 (52)
Pump beam waist (μm)	48	2	1•3
Total			22 (55)

The largest uncertainty in the σ_{2a} was from the beam waist. Since all optical components were stationary, the beam waist varied according to the beam divergence at the krypton laser. The beam waist measurement had an uncertainty

of about 4% due to the slightly distorted Gaussian beam profile. The maximum variation in the beam divergence was about 10~12% over the time of measurement for one data set (45 min.). The overall uncertainty in the σ_{2a} ranged between 0.2 to 0.5 x 10^{-20} cm^2. With a peak of the emission cross section 3.1 x 10^{-20} cm^2, the accuracy limit of our SPG measurement in the σ_{2a}/σ_e ratio varied from 6% to 16%.

The pump beam divergence was strictly an operating characteristics of our krypton laser. In this particular laser, a warm-up time of approximately four hours was required to reach reasonable optical stability. Some improvement in laser tube design has since been implemented by Coherent Radiation. The warm-up time in the new lasers with ceramic tube has been reduced to about 30 minutes. Therefore it is conceivable that the instability of the beam divergence might be significantly reduced. In alexandrite and emerald, the σ_{2a}/σ_e ratios were 14% and 20% respectively, near the peak of emission cross section. An accuracy of 6% in σ_{2a}/σ_e would generally be sufficient to determine the usefulness of other new tunable laser materials.

4. Laser Measurements

The first emerald laser was demonstrated in a flashlamp-pumped cavity (Appendix 3). The laser rod was made out of basically gem quality emerald, which had strong index of refraction gradient causing the beam breakup. The output energy was only 6.8 mJ at over 100J pump energy. The exceptionally high laser loss of 11%/cm was the primary cause for the low performance. However, no discoloration in the material was observed after hours of laser operation. Unlike many Cr doped Ga-garnets, emerald appeared to be color-center-free in flashlamp-pumped laser operation.

The optical quality of emerald has been improved steadily since the gem emerald days. However, the emerald crystals from Vacuum Ventures, Inc. are still limited in size. The complexity and the delicate balance in the crystal growth made the scale-up process non-trivial. Further flashlamp-pumped laser testing was postponed until high optical quality emerald of sufficiently large size was available.

Our focus in the laser measurements was on exploring the operating limits of in high quality emerald. Based on our experience with laser-pumped alexandrite lasers,[1] we continued to improve and optimize the laser cavity to attain laser photon conversion-limited performance. The laser oscillation was formed by two concave mirrors in a nearly concentric configuration. The emerald was pumped longitudinally through a dichroic mirror. The minimum beam waist of the laser standing wave was controlled by the mirror separation. This design offered the flexibility to attain matching of the pump beam waist with the laser cavity beam waist in the emerald sample. We tested an earlier emerald crystal in this cavity. A 38% output slope efficiency was measured, and the laser loss was 1.4% round trip in a 2.8 mm length sample, corresponding to a 2.4%/cm single-pass (Appendix 4). Results from laser measurements in the latest high quality emerald showed significant improvement. A 64% output slope efficienty was measured with an output coupler of 1.16% transmission at 768 nm. The maximum output power reached 1.65 watts with 3.6 watts of pump power and was pump power limited (Figure 4). These results are among the highest in efficiency reported in laser-pumped Cr lasers operating in quasi-cw mode. The calculated round trip laser loss 0.11% in a 3 mm length sample, corresponding to 0.36%/cm round trip. This laser loss did not include the ESA loss embedded in the total

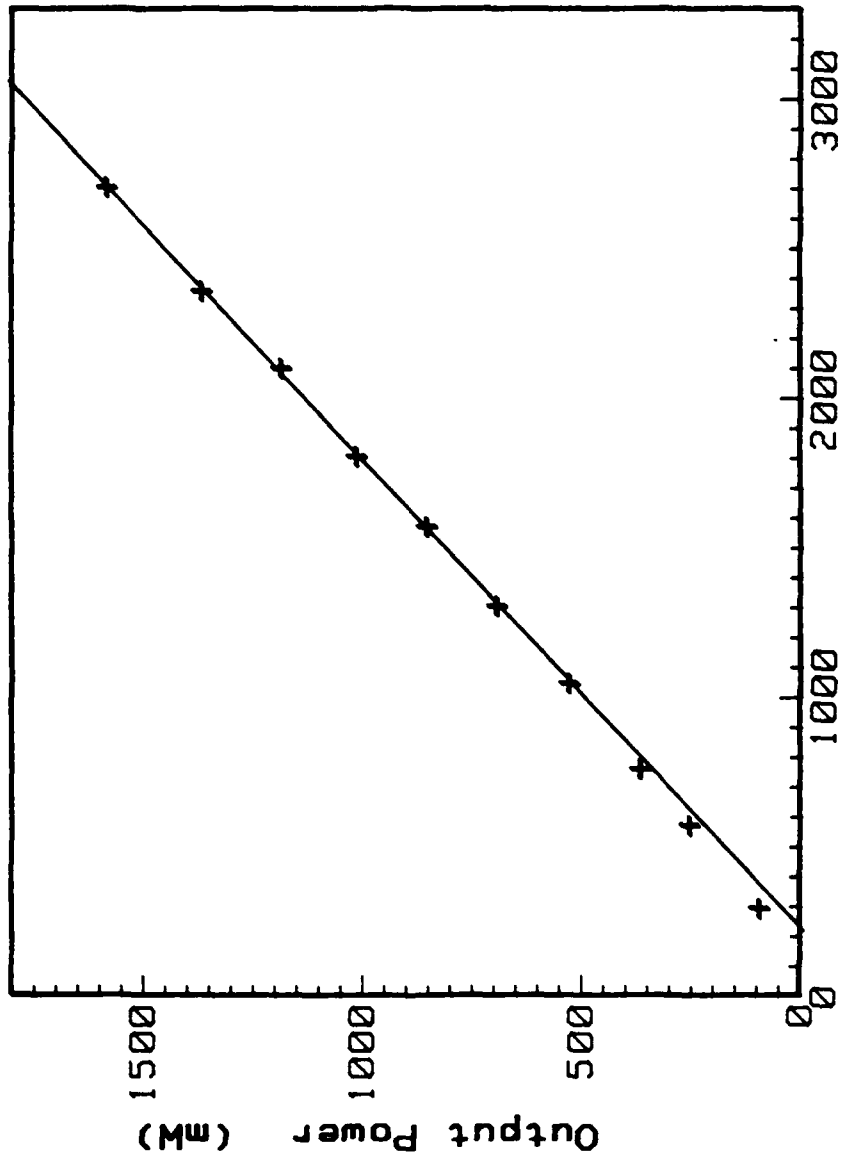

Figure 4. Emerald laser output as a function of absorbed pump power. The slope efficiency is 64% at 768 nm. The output coupler transmission was 1.16%.

laser loss measured from slope efficiency. If the ESA loss was included, for a comparison with the results obtained from the earlier emerald crystals, the total laser loss was 0.36%, which was about 4 times lower than that reported in Appendix 4. The laser quantum yield was 76%, which was slightly lower than a projected 85% in alexandrite[1]. With a single element birefringent filter, the emerald laser was tuned continuously from 720 nm to 842 nm. The lower bound was limited by the ground state absoption process as discussed earlier. Higher pump density would increase the gain population and deplete the ground state. Some extension in the shorter wavelength could be expected. However, operating at higher temperature would enhance the ground state absorption, and the tuning limit would shift towards longer wavelength. The long wavelength end of the tuning range was limited by the excited state absorption, and also to a small extent, by the optical losses in the crystal. Since the optical loss was already very low, extension of the long wavelength end of the tuning range is expected to be limited. In general, the emerald laser operated with high gain and high efficiency in the 750-790 nm range. In the 780-800 nm region, the emerald laser is likely to out-pe. form alexandrite.

The overall laser performance was limited by both the electronic loss and losses due to thermo-mechanical effects. Every contributing loss would lower the laser efficiency. To evaluate the emerald laser performance, we compare it to a number of room temperature Cr doped tunable lasers. Some of the laser-relevant spectroscopic parameters are listed in Table II. With the exception of GSGG and $KZnF_3$, all other laser measurements were made in our laboratory. Emerald has the second highest slope efficiency, second to alexandrite with a projected slope of 73% (51% was actually measured, with an estimated additional

Table II Summary of Spectroscopic Parameters in Cr-doped Room Temperature Tunable Lasers

	Alexandrite*	Emerald*	GSGG:Cr	$KZnF_3$:Cr	$ScBO_3$:Cr*	$SrAlF_5$:Cr*
Fluorescence peak wavelength (nm)	697	746	750	765	810	840
Laser tuning range (nm)	701-818	720-842	742-842	785-865	787-892	852-947
Lifetime at 22°C (μs)	260	60	114	80/270 (at 10K)	115	93
Peak emission cross section (10^{-20} cm^2)	0.7	3.1	0.8	--	1.2	2.3
Laser output slope efficiency (laser-pumped)	51%[1] (73%)	64%	28%[11]	14%[12]	29%[10]	3.6%[6]
σ_{2a}/σ_e (near minimum)	.14	.20	--	--	--	--

* Measurements were made in this laboratory.

22% leakage through the input coupler end). With the laser materials arranged in descending order of the crystal field strength at the Cr site, the slope values seem to indicate a trend of decreasing efficiency with decreasing crystal field. While the excited state absorption was only measured in alexandrite and emerald, a systematic study of the excited state absorption and correlating the result with the Cr electronic environment would likely lead to an understanding of the general principles of all Cr tunable lasers.

5. Some Refinements in Laser-pumped Laser Measurements

We demonstrated that the laser-pumped laser measurements, if done properly, can be used for a critical evaluation on laser performance. From the measurements in high optical quality alexandrite and emerald, we were confident that nearly 100% photon accountability could be attained in a finely tuned laser cavity. A sensitivity of 0.1% in the laser loss could be routinely measured in our setup. This is an important tool in monitoring the material progress in developing ultra-high quality laser crystals. Since the laser loss was based on the output slope efficiency, some caution must be taken in interpreting the results. In our early laser measurements[1] and by many other researchers working in this field, the loss L was deduced from an expression of the slope efficiency of:

$$\eta = \frac{h\nu_L}{h\nu_p} \frac{T_o}{T+L} \qquad (3)$$

where $h\nu_L$, and $h\nu_p$ are the laser photon and the pump photon energies respectively, T_o is output coupler transmission, T is the total transmission loss in the cavity. The loss term L consists of the intrinsic loss due to the excited state absorption, and an extrinsic loss due to the optical scattering, impurity absorption, stress-induced birefringence and thermal lensing effects. Equation

(3) also assumes no excited state absorption at the pump photon wavelength, which is not the case for most transition metal ion lasers at most pump wavelengths. We have incorporated the effect of the ESA processes, at both the ground state and the excited state and at both the laser photon energy and the pump photon energy[13] in the model. A modified version of the slope efficiency was derived and is given below:

$$\eta = \frac{h\nu_L}{h\nu_p} \quad \frac{T_o}{T+L+\Delta} \xi, \qquad (4)$$

where Δ is the excited state absorption loss at the laser wavelength, and ξ is given by:

$$\xi = \frac{N_1\sigma_a^p}{N_1\sigma_a^p + N_2\sigma_{2a}^p}, \qquad (5)$$

$$= \frac{N_1}{N_o+N_2\ (\sigma_{2a}^p-\sigma_a^p)}$$

where N_1 and N_2 are the Cr ion density at the ground state and excited state respectively, $N_o=N_1+N_2$ is the total Cr concentration, and the σ_a^p and σ_{2a}^p are the absoprtion cross sections of the ground state and the excited state at the pump wavelength respectively. The ξ factor accounts for the fraction of the absorbed pump power which contributes to the gain population N_2. In the case of emerald, σ_a^p and σ_{2a}^p are comparable[8]. With the parameters taken from the laser measurements in Figure 4, N_2 was 1% of N_o and ξ was 0.99. With high pumping density, N_2 can be 10~20% of N_o in long fluorescence lifetime materials. Depending on the pump wavelength, σ_{2a}^p/σ_a^p can be >>1. In that case, ξ will be significantly less than 1.

The excited state absorption term Δ in equation (4) consists of a product of the ESA cross section σ_{2a}, and the excited state ion density N_2. Therefore Δ varies with the overall loss in the laser. We developed a new approach to

measure the σ_{2a}/σ_e ratio from the laser results. This method provides an independent measurement of the σ_{2a} apart from the single-pass gain measurement. From equation (4), the slope efficiency is largely determined by the output coupler transmission T_o and the Δ term. With output coupler of different transmission coefficient, the output slope will change, so does the Δ. However, the L and ξ terms remain basically the same. Since T_o and η can be measured directly, the two Δ values can be used to deduce the ESA cross section σ_{2a}.

To relate the σ_e and σ_{2a} through the laser measurements we consider the threshold condition:

$$\begin{aligned} To+L &= (N_2\sigma_e - N_2\sigma_{2a} - N_1\sigma_a) \cdot 2l \\ &\simeq N_2 (\sigma_e - \sigma_{2a}) \cdot 2l \\ &\cong G - \Delta \end{aligned}$$

where we assume the ground state absorption loss is negligible at the laser photon energy, and we define G to be the stimulated emission gain $N_2\sigma_e$. We may also write

$$G = To+L+\Delta$$

and,

$$\frac{\sigma_{2a}}{\sigma_e} = \frac{\Delta}{G} \cdot$$

Since identical extrinsic loss L is assumed, we avoid any variation of insertion loss. One difficulty in this measurement was to have two output couplers both free running at the same wavelength. We were fortunate to have a pair of mirrors which had free running wavelengths at 776 nm and 777 nm, with output coupling of 1.76% and 0.608% respectively. The output slope efficiencies were 56.7% and 51% respectively. The σ_{2a}/σ_e ratio was calculated to be 38%, and the loss L was 0.11% in a 3 mm length emerald. The σ_{2a}/σ_a ratios at other free

running wavelengths were calculated using this L value. Laser output slopes were measured with a series of output couplers. The coupler transmission, the output slope, and the calculated σ_{2a}/σ_e values are summarized in Table III.

Table III. Output Slope Efficiency and the σ_{2a}/σ_e Ratios in Emerald.

Free running Wavelength (λ_L)	Output coupler Transmission (%)	Slope Efficiency (%)	σ_{2a}/σ_e
768	1.16	64	.20
771	0.85	56	.33
776	1.76	58.6	.38
777	0.608	51	.38
790	0.25	38.7	.54
822	0.89	38	.84

We would like to point out that the slope efficiency in emerald was in general very high. We measured a 38% slope even at 822 nm where the σ_{2a}/σ_e ratio approached 1. We have demonstrated high efficiency laser operation in emerald over a significant portion of its emission range. From figure (3), we expect the $\sigma_{2a}/\sigma e$ ratio to continue to increase toward shorter wavelengths. It is likely to reach a maximum around 755 nm. The laser loss is then dominated by the ground state absorption process and decreases at shorter wavelength.

The accuracy of $\sigma_{2a}/\sigma e$ ratio depended largely on the alignment of the laser oscillator and the coupling with the pump beam optics. Reproducibility in the slope efficiency was about 5% in our measurements. The accuracy can be improved by choosing output couplers with a larger difference in transmission coefficients. This method is more accurate in measuring larger $\sigma_{2a}/\sigma e$ ratios.

6. Emerald Crystal Growth

Emerald did not melt congruently, hence it could not be grown from the melt directly. There were two basic approaches to grow emerald crystals: flux growth

and hydrothermal growth. Both techniques were developed in the early sixties and synthetic emerald had since entered the jewelry market.

The flux technique has the advantage of ambient pressure. The most common flux has been $Li_2O \cdot MoO_3$ composition. Both Chatham and Gilson used the same flux to grow emerald. The main drawback was the slow growth rate. Typical growth period was 12 months to achieve about 1 cm growth. Other problems included trapping of flux, formation of phenacite, cracking, and optical nonhomogenious. While it is acceptable in the gem trade, the crystal quality is definitely not good enough for laser application.

Hydrothermal growth requires a more complicated growth apparatus. The crystal was grown under both high temperature (~ 600°C) and high pressure (over 12,000 psi). The choice of materials for the growth vessel was limited by the extreme nature of the growth. Techniques to grow emerald hydrothermally was developed by the Linde Division of Union Carbide. Despite the complexity of the growth evnironment, including the possibility of explosion due to stress corrosion if a leak occurs, hydrothermal growth offered superior crystal quality and faster growth rate.

6.1 Vacuum Ventures Emeralds

Currently Vacuum Ventures, Incorporated (VVI) is the only company in the U.S. commercially producing emerald by hydrothermal growth. VVI acquired the Union Carbide process and the equipment and has further perfected the growth technique. The basic growth process involves the dissolution of the proper nutrient material in a concentrated acid-salt solution and the growth on a beryl seed plate of a specific orientation. Typical growth time is about 1 month and a crystal of the size 50x12x6 mm^3 is harvested. We closely interacted with VVI

in the past three years and the crystal quality has improved significantly. Nevertheless, the VVI emerald growth has two basic limitations: First, the crystal is limited by its vessel size. The size mentioned above is about the limit for their equipment. Second, they use an isothermal growth environment with the nutrient ingredient fully dissolved in the solution. This approach lacks the control of the Cr distribution in the crystal.

6.2 Allied Emerald Crystal Growth Program

Our goal was to grow large size, high optical quality emerald for laser applications. Specific priorities were incorporated in the design of the hydrothermal growth apparatus. The growth proceeded in a steady state transport process. This ensured the uniformity of the overgrowth on the seed and a continuous growth for large crystals without concern about nutrient depletion. Our vessel volume during growth was built twenty times bigger than those of VVI. Special attention was given in ensuring the safety of personnel, including an emergency shutdown procedure which could be triggered by either temperature or pressure alarm. Since an accident explosion could cause not only physical damages but also health hazard due to the beryllium compounds, specific procedures were also developed for the confinement and cleaning of beryllium contamination. The vessels were operated inside a high pressure cubicle for protection. Thus far we tested 4 runs in our latest growth vessels without any incidents. Some emerald growth was attained in our vessel. The growth parameters are still being optimized.

6.3 Overall Results

Current cooperation with the VVI led to growth of high optical quality emerald. We established an in-house capability of emerald crystal growth.

Results from the initial growths are encouraging. We are continuing to modify the growth procedures. High optical quality emerald growth has been demonstrated in the VVI growths. With the availability of good quality seed plate of sufficient size, large good quality emerald is attainable with further development.

7. Summary and Conclusion

The electronic parameters of emerald lasers were characterized. Emerald has a peak emisison cross section of 3.1×10^{-20} cm^2 which makes emerald a high gain laser among Cr doped tunable lasers. The effect of the ground state and the excited state absorption processes on the laser tuning range and the laser efficiency was studied in detail. A laser-pumped single-pass gain measurement was developed. A 76% laser quantum yield was measured in emerald, lasing at 768 nm. The maximum attainable laser quantum efficiency was estimated to be about 84%. Emerald laser was tunable from 720 nm to 842 nm. High gain, high efficiency laser operation was observed from 760 nm to 790 nm. We have demonstrated that nearly 100% accountability in pump-photon conversion to laser-photon can be achieved in a highly efficient laser-pumped laser cavity. This cavity is also used for critical evaluation of other new laser materials such as $SrAlF_5:Cr$[6] and $ScBO_3:Cr$[10].

We also confirmed a number of negative results in favor of emerald lasers. We observed no anamolous absorption band such as those induced by color centers, charge-compensated ions or impurities, no nonradiative inequivalent Cr sites, and no nonhomogenious broading associated with the Cr level. The pump efficiency was nearly unity throughout the Cr^{3+} absorption band. Laser measurments also indicated nearly unity fluorescence efficiency.

The optical quality of emerald has been improved steadily under our crystal development program. The laser loss in the emeralds from the Vacuum Ventures, Inc. had reduced from 11%/cm to 0.4%/cm round trip. The optical nonhomogenious in the early day gem quality emerald was largely eliminated. However improvements in growth yield and crystal size are still to be achieved. In the Allied emerald growth program was a scale-up growth chamber was built, tested, and is now operational. Due to the constraints imposed by the nature of hydrothermal growth, progress was made slowly and cautiously. Four growth runs were completed and some emerald growth was attained. The growth parameters are still to be optimized. With the growth technology developed with Vacuum Ventures, Inc., the crystal quality and size are expected to continue to improve.

8. Reference

1. S.T. Lai, and M.L. Shand, "Highly efficient cw laser-pumped tunable alexandrite laser," J. Appl. Phys. vol. 54, pp. 5642-5644, 1983.

2. Neutron activation analysis was made in the department of nuclear engineering, North Carolina State University, Raleigh, NC.

3. T.H. Maiman, et al., "Stimulated optical emission in fluorescent solids. II Spectroscopy and stimulated emission in ruby," Phys. Rev. vol. 123, pp. 1151, 1981.

4. G.V. Gibbs, D.W. Breck, and E.P. Meagher," Structural refinement of hydrous and anhydrous synthetic beryl, $Al_2(Be_3Si_6)O_{18}$ and emerald, $Al_{1.9}Cr_{0.1}(Be_3Si_6)O_{18}$," Lithos vol. 1, pp. 275-285, 1968.

5. W.H. Fonger and C.W. Struck, "Temperature dependences of Cr^{3+} radiative and nonradiative transitions in ruby and emerald," Phys. Rev. B vol. 11, pp. 3251-3260, 1975.

6. H.P. Jenssen, and S.T. Lai, "Tunable-laser characteristics and spetroscopic properties of $SrAlF_5$:Cr," J. Optical Soc. America B, vol. 3, pp. 115-118, 1986.

7. M.L. Shand, "The quantum efficiency of alexandrite", J. Appl. Phys. vol. 54, pp. 2602, 1983.

8. W.M. Fairbank, Jr., G.K. Klauminzer and A.L. Schawlow, "Excited-state absorption in ruby, emerald and MgO:Cr^{3+}", Phys. Rev. B vol. 11, pp. 60-76, 1975.

9. M.L. Shand, J.C. Walling, and R.C. Morris, "Excited-state absorption in the pump region of alexandrite," J. Appl. Phys. vol. 52, pp. 953-955, 1981.

10. S.T. Lai, B.H.T. Chai, M. Long, and R.C. Morris, "$ScBO_3$:Cr-A room temtemperature near-infrared tunable laser," to be published , IEEE J. Quantum Electron. Oct. issue, 1986.

11. B. Struve and G. Huber, "Laser performances of Cr^{3+}:Gd(Sc,Ga) garnet," J. Appl. Phys., vol. 57, pp. 45-48, 1984.

12. U. Branch, and U. Durr, "Room temperature operation of the vibronic $KZnF_3$:Cr^{3+} laser," Optics Lett., vol. 9, pp 441-442, 1984.

13. S.T. Lai and M.L. Shand," Temperature dependence of gain in cw alexandrite laser," Proceedings of the International Conference on Lasers '83, pp 165-169, 1983.

9. List of Publications

1. M. L. Shand, and J. C. Walling, "A tunable emerald laser," IEEE J. Quantum Electron. vol. 18, pp. 1829-1830, 1982.

2. M. L. Shand, "The emerald laser," Proceedings International Conference in Lasers '82, STS Press, McLean, VA., 1982.

3. M. L. Shand, and S. T. Lai, " CW Laser-pumped emerald laser," IEEE J. Quantum Electron., vol. 20, pp. 105-108, 1984.

4. M. L. Shand, and S. T. Lai, "Laser-pumped single-pass gain," Springer Series in Optical Sciences, vol. 47, pp. 76-79, Springer-Verlag, NY., 1985.

5. S. T. Lai, "Review of spectroscopic and laser properties of emerald," Proceedings SPIE, The International Optical Engineering, vol. 622, "High power and solid-state lasers," pp. 146-150, 1986.

6. H. P. Jenssen, and S. T. Lai, " Tunable-Laser characteristics and spectroscopic properties of $SrAlF_5$:Cr," J. Optical Soc. America B, vol. 3, pp. 115-118, 1986.

7. S. T. Lai, B. H. T. Chai, M. Long, and R. C. Morris, "$ScBO_3$:Cr-A room temperature near-infrared tunable laser, " to be published, IEEE J. Quantum Electron. October issue, 1986.

10. Participating Scientific Personnel.

Shui T. Lai, Principal Investigator
Senior Research Physicist
Allied-Signal, Inc.

Micheal L. Shand
Manager, Laser Research and Development
Allied-Signal, Inc.

Bruce H. T. Chai
Research Associate
Allied-Signal, Inc.

Anthony G. Davis
Senior Research Techican
Allied-Signal, Inc.

Advanced degree earned: None.

11. Bibliography

Name: Lai, Shui T.

Education: M. S., 1975 and Ph. D., 1980 in Physics
University of Illinois, Urbana, Illinois

B. S. (Hon.) ,1972 in Physics
Chinese University of Hong Kong, Hong Kong

Position: Senior Research Physicist

Qualifications: Eleven years of experience in optics and solid state materials research.
Three patents, pending in new lasers and thin film display devices.

1982-1986
Allied-Signal, Inc.
Morristown, New Jersey

Characterization of new optical materials for applications in lasers and thin film CRT displays. Critical evaluation of new laser performence by spectroscopy and prototype laser testing. Search of new solid state lasers, contributing to the discovery of the $ScBO_3$:Cr and $SrAlF_5$:Cr lasers.

1980-1982
Research Associate
Department of Physics
University of Wisconsin, Madison, Wisconsin

Energy transfer and coherent two-photon absorption processes among rare earth ions in solids. Energy relaxation and lineshape studies in rare earths with high resolution, time-resolved spectroscopy.

1973-1980
Research Assistant
Department of Physics
University of Illinois, Urbana, Illinois

Raman and photoluminescence study of excitons in semiconductors. Raman scattering in electron-hole liquid in stressed Si, metal-insulator transition in heavily doped Si. Discovery of the Anderson-localized excitons in $GaAs_{1-x}P_x$.

Yale-in-China Scholar, 1973-1975

Lai, Shui T.
Page 2 of 3

Recent Publications

1. "High efficiency cw laser-pumped tunable alexandrite laser," S. T. Lai, and M. L. Shand, J. Appl. Phys., vol. 54, p. 5642, 1983.

2. "Q-switch cw pumped alexandrite laser," M. L. Shand, D. J. Harter, S. T. Lai, and H. Samelson, Proceedings International Conference on Lasers '83, p. 161, STS Press, Mclean, VA., 1983.

3. "Temperature dependence of gain in cw alexandrite laser," S. T. Lai, and M. L. Shand, Proceedings Internation Conference on Lasers '83, p. 165, STS Press, Mclean, VA., 1983.

4. "CW Laser-pumped emerald laser," M. L. Shand, and S. T. Lai, IEEE J. Quantum Electron., vol. 20, pp. 105-108, 1984.

5. "Photoluminecence study of excitons localized in indirect-gap $GaAs_{1-x}P_x$," S. T. Lai, and M. V. Klein, Phys. Rev. B, vol. 29, p. 3217, 1984.

6. "Study of localized excitons in indirect-gap $GaAs_{1-x}P_x$,"S. T. Lai, and M. V. Klein, J. Lumines., vol. 32/32, p. 482, 1984.

7. "Laser-pumped single-pass gain," M. L. Shand, and S. T. Lai, Springer Series in Optical Sciences, vol. 47, pp. 76-79, Springer-Verlag, NY., 1985.

8. "Review of spectroscopic and laser properties of emerald," S. T. Lai, Proceedings SPIE, The International Optical Engineering, vol. 622, "High power and solid-state lasers," pp. 146-150, 1986.

9. "Tunable-Laser characteristics and spectroscopic properties of $SrAlF_5$:Cr," H. P. Jenssen, and S. T. Lai, J. Optical Soc. America B, vol. 3, pp. 115-118, 1986.

10. "$ScBO_3$:Cr-A room temperature near-infrared tunable laser," S. T. Lai, B. H. T. Chai, M. Long, and R. C. Morris, to be published, IEEE J. Quantum Electron. October issue, 1986.

Patents

1. "Cr doped Gadolinium Scandium Aluminum garnet laser," S. T. Lai, M. L. Shand, and R. C. Morris, filed Feburary, 1984, patent pending.

2. "Multi-layer faceted luminescent screens," D. M. Qualtieri, and S. T. Lai, filed December, 1985, patent pending.

3. "Cr doped Scandium Borate laser," B. H. T. Chai, S. T. Lai, and M. Long, filed March, 1986, patent pending.

Name: Shand, Michael L.

Education: A.B. in Physics, 1968
Princeton University
Princeton, NJ

M.S., 1969 and Ph.D. in Physics, 1973,
University of Pennsylvania
Philadelphia, PA

Position: Manager
Security Clearance: SECRET, DOD

Qualifications: Seventeen years experience in optics research

1985-1986
Manager, Laser Research and Development
Allied-Signal, Inc.

Supervising over twenty professional and technical staff in the development of high brightness, high average power alexandrite lasers for applications in isotope separation, Lidar, and for the military.

1976-1985
Allied Corporation

Responsible for research on nonlinear optics in laser host crystals, single crystal and solution polymers, photoacoustic spectroscopy of several solid-state systems, Raman scattering in berlinite and polymers, laser physics and new solid-state laser crystals. In 1980, also an Adjunct Associate Professor of Physics at Stevens Institute of Technology, Hoboken, NJ.

1975-1976
Visiting Assistant Professor
Department of Physics
Arizona State University
Tempe, AZ

Teaching responsibilities and Raman scattering and phonon-phonon interactions in copper halides, in ionic conductors, and in ammonium halides.

1974
Research Associate
laboratoire de Physique des Solides
Universite Pierre et Marie Curie
Paris, France

Research on light scattering in liquid crystals.

Recent Publications

1. "Physical and optical properties of emerald," M.L. Shand, Invited paper in Optical Society of America 1984 Annual meeting, Technical program, OSA, p. 24, 1984.

2. "Review of tunable solid state laers," M.L. Shand, Appl. Optics, 1985.

3. "Design and performance of a 125 Hz, 50W alexandrite laser," R.C. Sam, W.R. Rapaport, M.L. Shand, Proceedings Southwest Conference on Optics, 1985, SPIE vol. 540, Washington, 1985.

4. "High power, high repetition rate, line narrowed alexandrite lasers," W.R. Rapaport, R.C. Sam, and M.L. Shand, Proceedings International Conference on Lasers '84, STS Press, McLean, VA 1985, p. 552.

5. Alexandrite laser technology," M.L. Shand, Proceedings of Scientific and Engineering Applications of Commercial lasers Devices, SPIE vol. 618, 1985, to be published.

Plus five other papers co-authored with, and listed under S.T. Lai.

Name: Chai, Bruce H.T.

Education: Ph.D. in Geochemistry, 1975
Yale University
New Haven, Connecticut

Position: Research Associate

Qualification: Over ten years research experience.
Author or co-author of 20 technical papers, and inventor or co-inventor of eight U.S. patents.

1977-1986
Allied-Signal Corporation.

Responsible for hydrothermal crystal growth program including the growth of berlinite ($AlPO_4$) and other quartz isomorphs, the growth of emerald crystals, the growth of rare earth polyphosphate crystals, synthesis and phase study of new compounds. Also responsible for the research on new laser crystals and nonlinear crystals.

1975-1977
Yale University
Post doctor research on kinetics of hydrothermal recrystallization of calcite and associated ion exchange as well as isotope exchange mechanism. Synthesis of rare earth carbonate, oxycarbonate crystals. Study on water interaction on silicate system under hydrothermal conditions.

Recent Publications

1. "Crystal Growth of $ScBO_3:Cr^{3+}$ - A New Near Infrared Tunable Laser Crystal", Proceedings, International Conference on Tunable Solid State Lasers, 1986. Springer series in Optical Sciences, Springer-Verlag, NY, to be published.

2. "Hydrothermal Growth of Berlinite (α-$AlPO_4$) Single Crystals," 2nd International Symposium on Hydrothermal Reactions, August, 1985.

Appendix 1.

Review of spectroscopic and laser properties of Emerald

S.T. Lai

Allied-Signal, Inc., Morristown, NJ 07960

Abstract

A summary of the laser-relevent spectroscopic properites and recent laser measurements in emerald are presented.

Introduction

Emerald ($Be_3Al_2Si_6O_{18}$:Cr) has beryl crystal structure with the Cr^{3+} laser active ions at the single octahedral site. The laser transition is from the Cr $^4T_2$ level to the ground state $^4A_2$. The vibronic coupling between the $^4T_2$ level and the host lattice provides for a Stoke-shift, which make emerald a four-level laser. The high oscillator strength between $^4T_2$ and $^4A_2$ transition derives from a lack of inversion symmetry of the highly distorted octahedron[1]. The emission cross sections for the sigma- and pi-polarizations are shown in Fig. 1. The peak of the emission cross section reaches 3.3×10^{-20} cm^2 at 746 nm, which is high among Cr doped tunable laser materials (Table I).

Fluorescence lifetime as a function of temperatures is shown in Fig. 2. The 60 μs lifetime decreases slowly with increasing temperatures to 250°C, beyond which the lifetime drops more rapidly. The slow lifetime variation below 250°C is understood to be due to the thermal population of the $^4T_2$ level, which has about three orders of magnitude higher oscillator strength to the ground state compared to that of the ^2E level. Above 250°C, multiphonon coupling provides for a nonradiative channel for the $^4T_2$ excited state ion relaxation to the $^4A_2$ ground state. Similar temperature dependence of the lifetime has also been observed in ruby and alexandrite.

Laser efficiency

Energy conversion efficiency is one of the important factors determining the usefulness of a laser. While there are fair selections of pump sources and laser cavity configurations to choose from to suit the particular spectroscopic character of laser materials, broad absorption bands such as those of Cr $^{3+}$ have been shown to be both efficient (for broadband pumping) and flexible (for diode or laser-pumping). The $^4T_2$ and $^4T_1$ bands in emerald cover significant portions of the visible spectrum (Fig. 3). The $^4T_2$ band shape definitely cannot

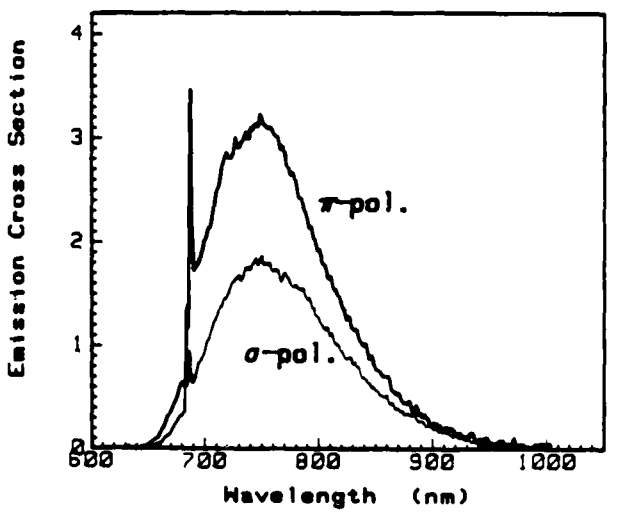

Fig. 1. Polarized emission cross sections σ_e of emerald at room temperature, in units of 10^{-20} cm^2.

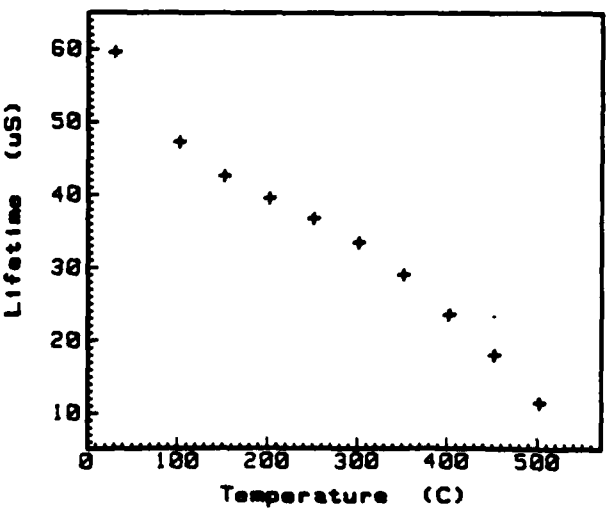

Fig. 2. Emerald fluorescence lifetimes as a function of temperature.

be fitted to the Huang and Rhys model with a single electronic level. We attribute this to a distribution of the oscillator strength in the phonon coupling among the $^4T_2$ multiplets. To evaluate the relative pump efficiency as a function of wavelength, polarized excitation spectra were measured and are shown in Fig. 4. Fluorescence at 760 nm was monitored while the excitation wavelength was scanned. We observed a nearly perfect match in the $^4T_1$ band and a better than 90% match in the $^4T_2$ band, indicating a nearly unity relative fluorescence efficiency throughout the absorption spectrum.

Laser measurements

Optical and thermal properties of emerald play a dominant role in its laser efficiency. Scattering loss due to crystal imperfections such as inclusions, residual strain from crystal growth, impurity absorption, and thermal lensing all tend to lower the quantum yield of a laser. The sum of all these effects can be deduced from the laser input versus output measurement. The power slope efficiency η can be expressed as[2]

$$\eta = \left(\frac{h\omega_L}{h\omega_P}\right) \frac{T_o}{T_o+L+\Delta} \cdot \xi, \qquad (1)$$

where L is the sum of the scattering losses discussed above, T_o is the output mirror transmission, the energy ratio in parenthesis accounts for the power conversion of laser photon energy (L) from the pump photon energy (P), and Δ is the excited state absorption loss at the laser wavelength. The factor ξ accounts for the absorption of the pump photons by ions at the excited states ($^4T_2$ and ^2E of Cr^{3+})

$$\xi = \frac{N_1\sigma_a(\omega p)}{N_1\sigma_a(\omega p) + N_2\sigma_{2a}(\omega p)}, \qquad (2)$$

where N_1 and N_2 are the ground state and excited state ion density, σ_a and σ_{2a} are the ground and excited state absorption cross sections at the pump photon energy $\hbar\omega p$. In emerald, the low threshold pump density kept the excited state ion density N_2 at a small fraction of the total ion density N_o due to the low scattering loss and small T_o values of the output couplers used in our measurements. With a 2 mm thick emerald in a nearly concentric cavity of about 20 cm in length, laser power outputs at the free-running laser wavelengths of 790 nm and 776 nm with two output couplers of 0.25% and 1.75% transmission respectively are shown in Fig. 5. The output power slope efficiencies are 39% and 51%

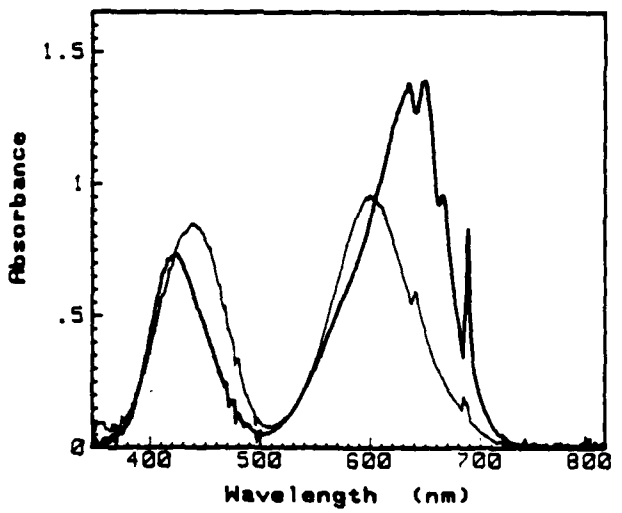

Fig. 3. Polarized absorption spectra of emerald. The π- and σ- polarized spectra are the heavy and light curves respectively.

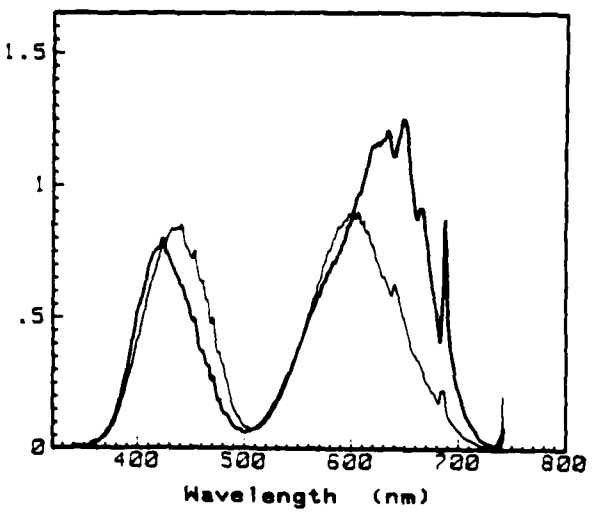

Fig. 4. Polarized excitation spectra of emerald. The π- and σ-polarized spectra are the heavy and light curves respectively.

Table I. Summary of spectroscopic parameters in Cr-doped room temperature tunable lasers

	Alexandrite	Emerald	GSGG:Cr	$KZnF_3$:Cr	$ScBO_3$:Cr	$SrAlF_5$:Cr
Fluorescence peak wavelength (nm)	697	746	750	765	810	840
Fluorescence spectrum FWHM (nm)	662-735	682-798	720-820	740-835	755-890	777-937
Laser tuning range (nm)	701-818	720-842	742-842	785-865	787-892	852-947
Lifetime at 22°C (μs)	260	60	114	80/270 (at 10K)	115	93
Peak emission cross section (10^{-20} cm^2)	0.7	3.3	0.8	--	1.2	2.3
Laser output slope efficiency (laser-pumped)	51%(3)	51%*	28%(4)	14%(5)	29%(6)	3.6%(7)

* Present Work

respectively. Output power in excess of 600 mW was measured at 1.6 watts of absorbed power. These results demonstrate highly efficient laser operation in emerald. From the 39% slope efficiency at 0.25% mirror transmission, we can estimate the laser losses from Equations (1) and (2). At a 60 μm pump beam waist (radius), and a 150 mW of threshold pump power, the exicted state ion density N_2 was calculated to be about 1% of the total Cr ion density in the crystal. The excited state absorption cross section in emerald at the pump wavelength (647.1 nm) is comparable to the ground state absorption cross section at the pump wavelength[8]. The factor ξ can be reduced to

$$\xi = \frac{N_1}{N_o + N_2[\sigma_{2a}(\omega p) - \sigma_a(\omega p)]} \approx \frac{N_1}{N_o} \qquad (3)$$

where $N_o = N_1 + N_2$, the Cr density in the sample. Hence ξ is 0.99 in our case. With T_o=0.25%, the sum L+A is 0.28% round trip loss in the 2 mm long sample. Using the result from the single-pass gain measurement (next section), we can isolate the effect of excited state absorption A, and calculate, L to be 0.074%, or 0.34%/cm round trip. This loss value is comparable to the best of well developed solid state laser materials such as alexandrite and YAG.

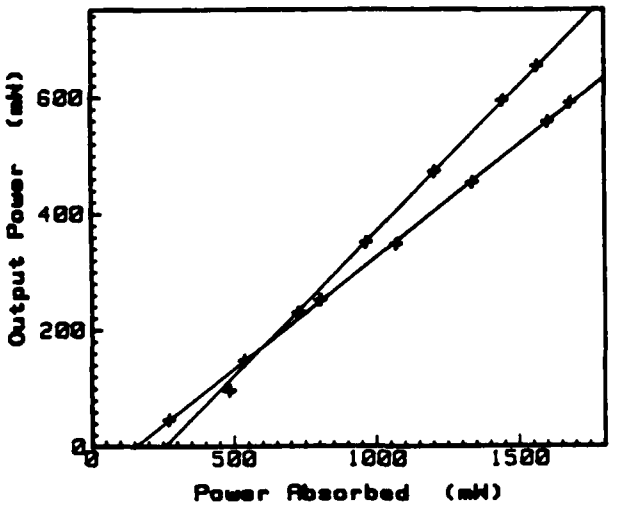

Fig. 5. Emerald laser output versus absorbed pump power. The 51% and 39% slopes were measured with 1.75% and 0.25% output couplers respectively.

Excited state absorption

At the pump wavelength, the effect of the excited state absorption on the laser performance has been pointed out in the last section. It is clear that even though σ_{2a} and σ_a are comparable, the output efficiency is only slightly modified by the depopulation of the ground state in the case of low threshold (Eq. 3). However, if the excited state absorption cross sections are comparable at the laser wavelength, high threshold and low output power slope efficiency can be expected and laser oscillation may not even be attainable due to the additional laser loss L discussed earlier. While some of the contributing components in the laser loss L can be reduced or eliminated by improved crystal quality, and by optimization of the heat dissipation scheme in the laser, the excited state absorption is intrinsic to the laser material and could place an ultimate limit on the laser efficiency.

A laser-pumped single-pass gain method has been developed to measure the excited state absorption cross sections σ_a at the laser wavelengths. Excited state ion density was maintained by focussing a laser beam (pump source) into a small cross sectional area. Since the profile of the laser beam is well defined and can be fairly accurately measured, the excited state density can be easily calculated from the absorbed pump power, while the same task is non-trivial, if not impossible, in a lamp-pumping setup.[9] Another advantage of the laser-pumped scheme is the small sample size required for the measurement. Significant time and resources may be saved if samples of few millimeters thick instead of a 5 ~ 6 cm long laser rod are used in the survey of new laser materials.

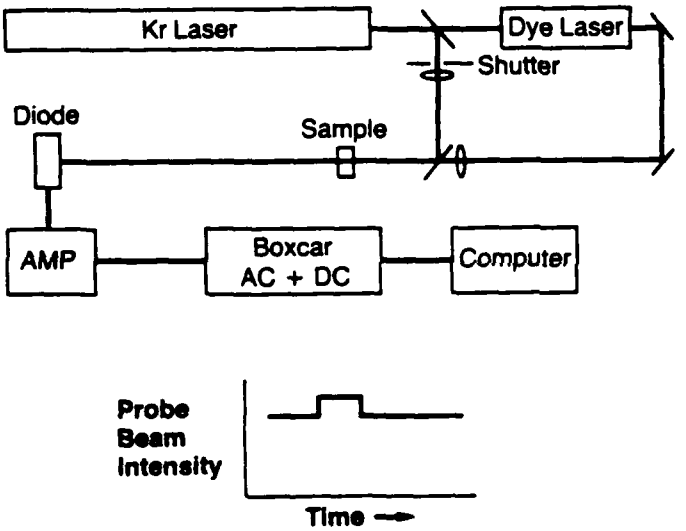

Fig. 6. Schematic of the single-pass gain measurement. The probe beam intensity showed a gain in the time window when the emerald was pumped (shutter open).

A schematic of the experimental setup is shown in Fig. 6. A krypton ion laser was used as the pump source for both the laser gain medium and a dye laser. The output of a dye laser (probe beam) was tuned to the gain wavelengths of emerald. The pump beam and the probe beam were aligned to be colinear and overlapping in the emerald sample. The pump arm was modulated by a mechanical shutter. The probe beam, detected by a silicon diode, showed a corresponding gain, or loss at the time intervals in which the emerald was pumped. The ratio of probe intensity when the sample was pumped to the probe intensity when pump was blocked is the single-pass gain (SPG) to be measured. A detailed analysis relating the SPG to the emission cross section σ_e, the ground state absorption cross section σ_a, and the excited state absorption cross section σ_{2a} at the laser wavelengths can be found in the earlier report[10].

Results of the SPG measurements from Ref. 10 are included in Fig. 7. The excited state absorption cross sections as a function of wavelengths were calculated using an expression from Ref. 10, assuming a 100% fluorescence quantum yield, and are shown in Fig. 8. Hence the calculated σ_{2a} in Fig. 8 represents upper-bound values. The σ_{2a}/σ_e ratio is higher in emerald than in alexandrite at most laser wavelengths[10]. However the net cross section (σ_e-σ_{2a}) in emerald is higher due to its larger emission cross sections.

Acknowledgement

We would like to thank B.H.T. Chai and R.C. Morris for many useful discussions. This work is supported by the U.S. Army Research Office, Research Triangle Park, NC, under a grant DAAG 29-83-C-0015.

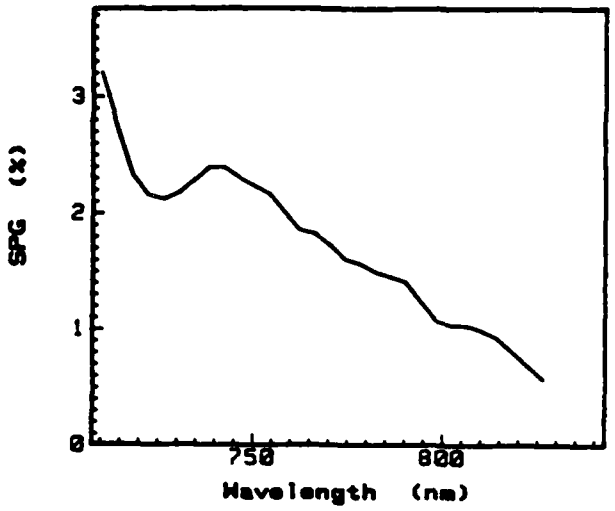

Fig. 7. The single-pass gain values of the probe beam as a function of wavelength . The E-field of the probe is parallel to the c-axis.

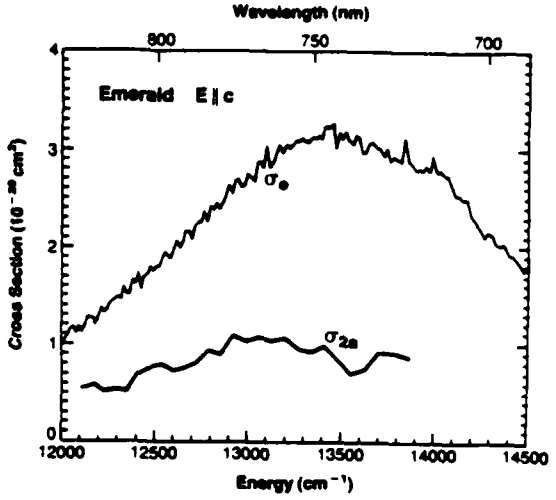

Fig. 8. The calculated excited state absorption cross sections σ_{2a} from SPG measurements. The σ_e spectrum is included for comparison. Both spectra are π-polarized.

References:

1. Morosin, B., "Structure and thermal expansion of beryl," Acta Cryst. vol. B28, pp. 1899-1902, 1972.

2. Lai, S.T. and Shand, M.L., "Temperature dependence of gain in cw alexandrite lasers," Proceedings of International Conference on Lasers '83, pp. 165-169, 1983.

3. Lai, S.T., and Shand, M.L., "High efficiency cw laser-pumped tunable alexandrite laser," J. of Appl. Phys. vol. 54, pp. 5642-5644, 1983.

4. Struve, B. and Huber, G., "Laser performance of Cr^{3+}:Gd (Sc,Ga) garnet," J. Appl. Phys. vol. 57, pp. 45-48, 1984.

5. Branch, U., and Durr, U, "Room temperature operation of the vibronic $KZnF_3:Cr^{3+}$ laser," Optics Letters, vol. 9, pp. 441-442, 1984.

6. Lai, S.T., Chai, B.H.T., Long, M., and Morris, R.C., "$ScBO_3$:Cr-A room temperature near-infrared tunable laser," IEEE J. Quantum Electronics, to be published.

7. Jenssen, H.P., and Lai, S.T., "Tunable-laser characteristics and spectroscopic properties of $SrAlF_5$:Cr." J. Optic. Soc. Am. vol. B3, pp. 115-118, 1986.

8. Veremeichik, T.F., "Similarity of ground- and excited-state absorption spectra of Cr^{3+} ions in a strong crystal field," Phys. Stat. Solid.(b), vol. 124, pp. 719-729, 1984.

9. Huang, J.W., and Moos, H.W., "Absorption spectrum of optically pumped $Al_2O_3:Cr^{3+}$," Phys. Rev. vol. 173, pp. 440-444, 1968, and Shand, M.L., and Walling, J.C., "Excited-state absorption in the lasing wavelength region of alexandrite, "IEEE J. Quantum Electron. vol. QE-18, pp. 1152-1155, 1982.

10. Shand, M.L., and Lai, S.T., "Laser pumped single pass gain," Tunable Solid State Lasers, Springer Series in Optical Sciences vol. 47, pp. 76-79, 1985.

Appendix 2.

Laser Pumped Single Pass Gain

M.L. Shand and Shui T. Lai
Applied Corporation, Corporate R&D, Morristown, NJ 07960, USA

Laser pumped single pass gain measurements are particularly useful for small samples and are sufficiently accurate to determine excited state absorption cross-sections in solid state tunable laser materials. Preliminary results for alexandrite and emerald are presented.

1. Introduction

Flashlamp pumped single pass gain (SPG) measurements have been used to determine the excited state absorption cross-section, σ_{2a}, of Cr^{3+} throughout the vibronic lasing region of alexandrite [1]. The wavelength dependence of σ_{2a} together with the emission cross-section, σ_e, and the ground state absorption cross-section, σ_a, have been used to model alexandrite laser performance [2]. Two problems arise in applying this technique to new potential laser materials. First, the sample must be available in sufficient size to make rods of at least one to two inches long. Second, a method for determining the excited state ion density must be found. For the alexandrite measurements, the decrease in the sharp R line ground state absorption was used to determine the percentage of Cr^{3+} ions in the excited state. Many of the Cr^{3+} laser hosts discussed in these proceedings [3] do not have measurable R line absorption.

The laser pumped SPG measurement overcomes both these problems. First, the sample length needed is only a few mm because of the strong and localized absorption of the pump light. Second, the number of excited state ions can be calculated from the measured absorbed pump light. These features of the laser pumped SPG measurement will be demonstrated in the experiments described below. The results are preliminary, however, they show that σ_{2a} can be extracted from these experiments.

2. Experiment and Analysis

A 647 nm Kr laser line pumps both the sample and a dye laser, which provides a probe beam. The pump beam is chopped, typically on for 1-5 ms at 10-20 Hz, to reduce heating in the optics and in the sample. The probe beam is coincident with the pump beam, with the overlap monitored by observing the thermal lensing experienced by the probe beam. The pump and probe beam are focussed at the sample position. The probe beam power has a dc component representing the power of the transmitted beam through the unpumped sample and an ac component representing the power increase or decrease (gain or loss) of the transmitted beam through the pumped sample. The ratio of probe beam power with pumping to probe beam power with no pumping, P_p/P_u, is given by $1+P_{ac}/P_{dc}$. The probe beam intensity is kept sufficiently low to avoid gain saturation. The maximum gain is less than 2% so that parasitic losses such as amplified spontaneous emission can be ignored.

The excited state ion density can be calculated from the absorbed pump power. Excited state absorption consumes part of the pump photons. A correction for the pump beam excited state absorption is made by measuring the SPG as a function of pump power. At low powers the SPG is proportional to pump power. At high powers, the SPG is less than linear with pump power, as part of the pump light contributes to excited state absorption. Extrapolation of the linear portion of SPG vs pump power gives the expected SPG if no excited state absorption of the pump were present. This expected value of SPG is used in the analysis of the data.

The analysis is based on the fact that both the probe and pump beams and therefore the excited state ion density, $N_2(r)$, have Gaussian spatial profiles [4]. The probe beam intensity after the sample for the two cases of the sample pumped, $I_p(r)$, and of the sample unpumped, $I_u(r)$ are given by

$$I_p(r) = I_o(r)\exp[N_2(r)(\sigma_e-\sigma_{2a}+\sigma_a)\ell-N\sigma_a\ell-L] \quad (1)$$

$$I_u(r) = I_o(r)\exp[-N\sigma_a\ell-L] \quad (2)$$

where ℓ is the sample length, N is the total Cr^{3+} ion density, and L accounts for the scattering losses in the sample and on all optical surfaces.

The exponential factor in (1) is generally small, thus the exponential function can be expanded in a power series. Taking the series to second order and integrating (1) and (2) over the beam area gives the power of the probe beam in the two cases. The resulting ratio is

$$P_p/P_u = 1 + \frac{2(\sigma_e-\sigma_{2a}+\sigma_a)\alpha P_{pump}\tau}{h\nu_{pump}\pi(\omega^2_{pump} + \omega^2_{probe})} + \frac{2(\sigma_e-\sigma_{2a}+\sigma_a)^2\ (\alpha P_{pump}\tau)^2}{(h\nu_{pump}\pi\omega_{pump})^2(\omega^2_{pump}+2\omega^2_{probe})} \quad . \quad (3)$$

Note that this expression depends neither on sample length nor on Cr^{3+} concentration in the sample.

The value of σ_{2a} is obtained from (3) as all the other parameters can be either measured or calculated. P_p/P_u is the SPG result, σ_e and σ_a are determined from fluorescence measurements and the extended McCumber theory [1], and the beam waists are determined from the beam divergence which is measured with a diode array.

3. Results and Discussion

The apparatus has been tested with alexandrite, for which σ_{2a} is known [1]. The calculated σ_{2a} are shown in Fig. 1. The probe beam was polarized parallel to the b axis of alexandrite, which is the only polarization direction showing gain. The values of σ_a are very close to those measured previously with flashlamp pumping.

The results for emerald are shown in Fig. 2 for polarizations parallel and perpendicular to the hexagonal axis (c axis). The ratio of σ_{2a} to σ_e for emerald in the gain region for E//c is comparable to that of alexandrite. The σ_{2a} for both polarizations are comparable, so that for E⊥c, σ_{2a} is a significant fraction of σ_e. This result implies that the E⊥c direction may not be as useful for lasers as previously expected.

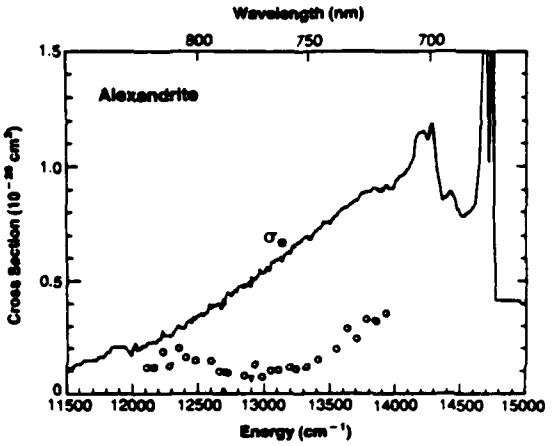

Fig. 1 Emission cross-section (solid-line) and excited state absorption cross-section (circles) for alexandrite E//b

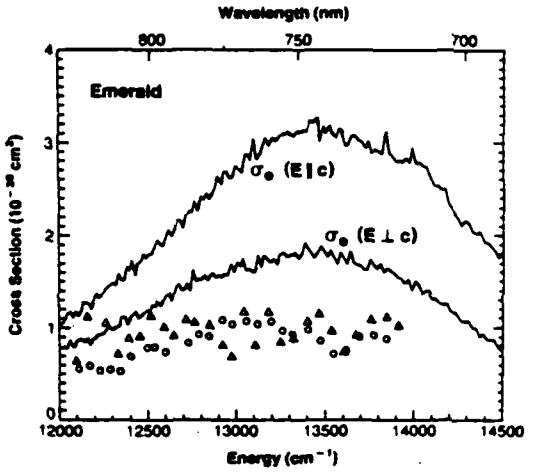

Fig. 2 Emission cross-section for emerald, polarization E//c and E⊥c (solid lines); excited state absorption cross-section E//c (circles) and E⊥c (triangles)

The major source of error in determination of σ_{2a} is in determining the beam waists. The main difficulty is that the Kr laser takes a long time (>35 hours) to reach thermal equilibrium. During this time the pump beam waist changes by over 25%. The probe beam waist is relatively stable and is also smaller than the pump beam waist by a factor of three to limit thermal lensing effects, so that the pump beam waist error dominates the error in σ_{2a}. Efforts are now underway to improve the pump beam waist stability. *Until these efforts are complete, these results must be considered* preliminary.

5. Conclusion

The laser pumped SPG measurement can be used to determine σ_{2a}. The system has been tested with alexandrite and used to determine σ_{2a} in emerald. The major problem at the moment is stability of the pump source.

6. Acknowledgements

We thank R.C. Morris and H.P. Jenssen for helpful discussions. This project is supported in part by the U.S. Army Research Office, Research Triangle Park, NC.

References

1. M.L. Shand and J.C. Walling, IEEE J. Quantum Electron. QE-18, 1152, 1982; M.L. Stand and H.P. Jenssen, IEEE J. Quantum Electron. QE-19, 480, 1983.

2. R.C. Sam, these proceedings; D.F. Heller and J.C. Walling, Conference on Lasers and Electro-Optics 1984, Opt. Soc. of Amer., p. 102.

3. G. Huber and K. Petermann, these proceedings.

4. S.T. Lai and M.L. Shand, J. Appl. Phys. 54, 5642 (1983).

Appendix 3. -46-

A Tunable Emerald Laser

MICHAEL L. SHAND AND JOHN C. WALLING

Abstract—Emerald is a new broadly wavelength-tunable vibronic laser material with stimulated emission in the red to infrared due to $^4T_2 \rightarrow {}^4A$ transitions of Cr^{3+}. Emerald has gain from 12 050 cm^{-1} to 14 000 cm^{-1} with high gain from about 12 300 cm^{-1} to 13 700 cm^{-1}. An emerald laser oscillator has been achieved, but has high losses.

EMERALD ($Be_3Al_2(SiO_3)^6:Cr^{3+}$), a chromium-doped beryl with hexagonal crystal structure, is a new tunable vibronic laser. The laser gain is due to transitions from the $^4T_2$ level to the vibronically excited ground state of Cr^{3+}. Unlike many previous vibronic lasers [1]-[5], emerald, like alexandrite [6], operates at room temperature. The single pass gain (SPG) of emerald has been measured from 12 000 cm^{-1} (835 nm) to 14 400 cm^{-1} (695 nm). High gain is present over the central portion of this region. Furthermore, an emerald laser oscillator has been operated, and tunability has been demonstrated.

The SPG of emerald is shown in Fig. 1 for two polarizations. The SPG apparatus has been described previously [7]. A probe beam traverses the sample rod which is in a flashlamp cavity with an 80 μs pulse width. The intensity of the probe beam is measured at two times: 1) the flashlamp is on and the rod is pumped (I_p), and 2) the flashlamp is off and the rod is unpumped (I_u). $I_p = I_o t^2 \exp(g_p l)$ and $I_u = I_o t^2 \exp(g_u l)$ where I_o is the intensity before the rod, t is the transmission at the ends of the rod, l is the rod length, and g_p (g_u) is the gain in the pumped (unpumped) case. The data in Fig. 1 are $\Delta G = g_p - g_u = [\ln(I_p/I_u)/l]$ with a total flashlamp energy of 170 J. The rod has approximately 1.5 atm percent Cr^{3+} with respect to the Al sites and has the hexagonal c axis at 45° to the rod axis so that one polarization direction corresponds to $E \perp c$ and the other polarization to equal combinations of $E \perp c$ and $E \parallel c$.

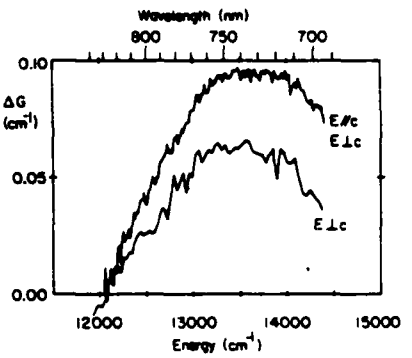

Fig. 1. Single pass gain of emerald for two polarization directions.

The data in Fig. 1 allow an estimate of the maximum emission cross section σ_e for $E \parallel c$. $\Delta G(E \perp c) = 0.065$ cm^{-1} and $\Delta G(E \perp c + E \parallel c) = 0.93$ cm^{-1}, so that $\Delta G(E \parallel c) = 0.12$ cm^{-1}. Furthermore,

$$g_p = cN^+(\sigma_e - \sigma_{ia}) - c(1 - N^+)\sigma_a$$
$$g_u = c\sigma_a \qquad (1)$$

where c is the Cr^{3+} concentration in ions/cm^3, N^+ is the frac-

Manuscript received June 18, 1982.
M. L. Shand is with Corporate R&D, Allied Corporation, Morristown, NJ 07960.
J. C. Walling is with Electro-Optical Products, Allied Corporation, Warren, NJ 07060.

0018-9197/82/1100-1829$00.75

tion of ions in the excited state, σ_{2a} is the excited state absorption cross section, and σ_a is the ground state absorption cross section. The ground state absorption has been measured in this energy region; σ_a is negligibly small at energies less than 13 600 cm^{-1}. Measurement of the excited state absorption in alexandrite ($BeAl_2O_4:Cr^{3+}$) shows that σ_{2a} is small near 13 500 cm^{-1}. Assuming that the same is true for emerald, and that the fraction of excited ions is 9 percent, which is based on the fact that a similarly doped alexandrite rod of the same length as this emerald rod and in the same flashlamp cavity had a 15 percent excitation level for 1.6 times more pump energy, then $\sigma_e = \Delta G/cN^+ \approx 0.12\ cm^{-1}/(9.2 \times 10^{19}\ cm^{-3} \cdot 0.09) = 1.4 \times 10^{-20}\ cm^2$. The maximum σ_e of emerald is therefore estimated at two times the σ_e of alexandrite. This rough estimate is consistent with the relation of the measured SPG for alexandrite and emerald. The maximum SPG for the alexandrite rod above with flashlamp energy of 280 J was $\Delta G \approx 0.08\ cm^{-1}$, which again implies that the gain of an appropriately oriented emerald rod would be approximately twice that of the alexandrite rod for the same condition.

A laser oscillator has been made with a 19 × 4 mm diameter rod, again with the c axis at approximately 45° to the rod axes. The rod was mounted in the same water-cooled ceramic flashlamp cavity used in the SPG measurements. The optical cavity was formed with a high reflector and a 95 percent reflectivity output coupler. Both mirrors were concave with a 4 m focal length. The laser emitted 6.8 mJ at 757.4 nm. With output mirrors having different reflectivity spectra, the laser operated at wavelengths from 751.1 to 759.2 nm.

The laser has large losses ($\simeq 0.11\ cm^{-1}$), presumably due to the beam breakup which is caused by planes in the crystal having slightly different indexes of refraction. Each of these growth planes along which the index of refraction is constant is parallel to the others and perpendicular to the direction of fastest crystal growth. Beam breakup is caused by reflection from these planes, and can be observed by passing a probe beam through the crystal. The losses can be minimized by directing the probe beam parallel to these planes. The laser rod described above was cut with the rod axis approximately parallel to these planes.

In summary, emerald exhibits gain from 12 050 to 14 000 cm^{-1} with fairly high gain from 12 300 to 13 700 cm^{-1}. A tunable laser has been made which, however, has large losses due to beam breakup.

Acknowledgment

The authors acknowledge the technical assistance of A. G. Davis and thank R. C. Morris and J. Riesenfeld for comments on the manuscript.

References

[1] L. F. Johnson, H. J. Guggenheim, and R. A. Thomas, "Phonon-terminated optical lasers," *Phys. Rev.*, vol. 149, pp. 179–185, 1966.

[2] L. F. Johnson, R. E. Dietz, and H. J. Guggenheim, "Optical maser oscillation from Ni^{2+} in MgF_2 involving simultaneous emission of phonons," *Phys. Rev. Lett.*, vol. 11, pp. 318–320, 1963.

[3] —, "Spontaneous and stimulated emission from Co^{2+} ions in MgF_2 and ZnF_2," *Appl. Phys. Lett.*, vol. 5, pp. 21–23, 1964.

[4] L. F. Johnson and H. J. Guggenheim, "Phonon-terminated coherent emission from V^{2+} ions in MgF_2," *J. Appl. Phys.*, vol. 38, pp. 4837–4839, 1967.

[5] P. F. Moulton and A. Mooradian, "Divalent transition-metal solid state lasers," *IEEE J. Quantum Electron.*, vol. QE-17, p. 140, Feb. 1981.

[6] J. C. Walling, O. G. Peterson, H. P. Jenssen, R. C. Morris, and E. W. O'Dell, "Tunable alexandrite lasers," *IEEE J. Quantum Electron.*, vol. QE-16, pp. 1302–1315, Dec. 1980.

[7] M. L. Shand and J. C. Walling, "Excited-state absorption in the lasing wavelength region of alexandrite," *IEEE J. Quantum Electron.*, vol. QE-18, pp. 1152–1155, July 1982.

Appendix 4. -48-

CW Laser Pumped Emerald Laser

MICHAEL L. SHAND AND S. T. LAI

Abstract—A CW laser pumped emerald laser is reported. A 34 percent output power slope efficiency is observed with longitudinal pumping by a krypton laser in a nearly concentric cavity. The laser has been tuned from 728.8 to 809.0 nm. Losses in emerald are larger than those of alexandrite determined in a similar cavity. Our data also indicate that the excited state absorption minimum is shifted from that of alexandrite.

I. Introduction

EMERALD [$Be_3Al_2(SiO_3)_6:Cr^{3+}$] is a tunable vibronic laser [1] due to transitions of the Cr^{3+} ion. The emission cross section (σ_e) of emerald [2] is approximately four times larger than that of alexandrite ($BeAl_2O_4:Cr^{3+}$), a previously discovered [3] and well-studied [4], [5] vibronic laser. Emerald also has lasing action at the wavelength of the R line emission [6] which is presumably a nonvibronic three-level process. σ_e is larger in emerald than in a number of other known Cr^{3+} vibronic lasers such as garnets [7], [8] and is comparable to that in several low crystal field materials which have not lased, such as phosphates [9].

Emerald lasers have been achieved with pumping by flashlamps [1] and by short laser generated pulses [6]. In this letter a CW laser pumped emerald laser is described. The experimental arrangement and results are presented in the next section which is followed by a discussion of the results.

II. Experiment and Results

The experimental setup [4] is shown in Fig. 1. An emerald sample [Fig. 1(f)] of length 2.8 mm with cross section 3.8 × 5.1 mm with 1.8 atm percent Cr was pumped longitudinally by a CW laser at 647.1 nm. The 2.8 mm axis was chosen parallel to the crystal growth direction to avoid pump beam break-

Manuscript received June 20, 1983; revised October 10, 1983. This work was supported in part by the U.S. Army Research Office, Research Triangle Park, NC.

The authors are with Corporate Research and Development, Allied Corporation, Morristown, NJ 07960.

0018-9197/84/0200-0105$01.00

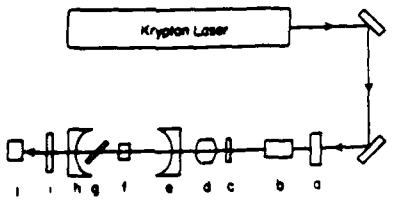

Fig. 1. Schematic diagram of the laser experiment. The pump beam (647.1 nm) is directed through a light chopper (a), polarization rotator (b), a neutral density filter (c), a focusing lens (d), input coupler mirror (e), the gain specimen (f), a birefringent filter (g), an output mirror (h), a long wave pass color filter, Schott RG-9 (i), and a diode (j).

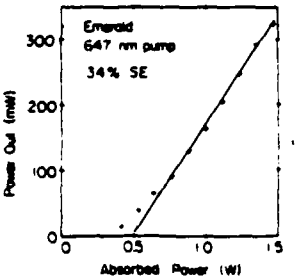

Fig. 2. CW output power versus absorbed pump power of the emerald laser.

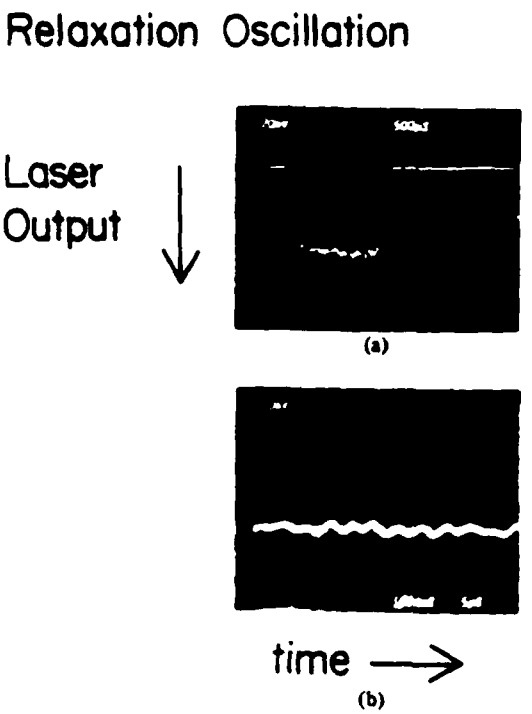

Fig. 3. The time dependence of the emerald laser output: (a) output at pump pulse duration (500 μs/cm); (b) output on an expanded time scale (5 μs/cm).

up [1]. The pump beam passed through a chopper [Fig. 1(a)] to reduce heating effects. Most of the results reported here were obtained with a duty factor (i.e., duration between chopper openings divided by duration of chopper opening) of 125. Without the chopper, sample heating was observed in the form of decreasing or unstable laser output. At a 60 μm pump beam waist in the sample, stable operation was reached after a few seconds to tens of seconds depending on the absorbed pump power. Emerald is a negative uniaxial crystal; in our sample the optic axis (*c*-axis) was approximately 60° from the direction of propagation (the 2.8 mm length). The polarization of the pump beam was adjusted by the polarization rotator [Fig. 1(b)] to yield maximum absorption in the sample which is parallel to the 5.1 mm edge. The polarization direction corresponds to the maximum projection of the electric field onto the *c*-axis. The laser output is polarized in the same direction. The pump and laser beams are therefore extraordinarily polarized and the path length in the sample is greater than the physical thickness. However, $(n_e - n_o)/n_o$ is only -2.6×10^{-3} so the additional path length can be ignored. The sample transmission is 24.1 percent at 647.1 nm. A neutral density filter [Fig. 1(c)] allowed output power slope efficiency measurements. The pump beam waist in the sample is determined by the position and focal length of the achromat lens [Fig. 1(d)] and was measured using a microscope. The input coupler [Fig. 1(e)] is a 5 cm radius high reflector (99.5 percent) at 765 nm with good transmission at 647.1 nm. The output coupler [Fig. 1(h)] has a 5 cm radius with 98.8 percent transmission at 765 nm. The laser cavity is nearly concentric to allow the cavity mode to be adjusted by changing the cavity length. The pump laser beam was stopped by a long wave pass Schott filter RG-9 [Fig. 1(i)]. The laser output power was detected by a diode [Fig. 1(j)] and measured with a boxcar integrator.

The laser output power as function of absorbed pump power is shown in Fig. 2. The output laser wavelength was 765 nm and was polarized parallel to the 5.1 mm sample edge, which contains a projection of the *c*-axis. The data were taken at a fixed cavity length which corresponds to a cavity mode of 60 μm. The divergence of the emerald laser was measured and also corresponds to a 60 μm beam waist. The pump beam waist was adjusted to 60 μm by changing the focusing lens position. Optimized performance in this cavity has been shown to be achieved with pump beam waist and laser beam waist equal [4]. An output slope efficiency of 34 percent and threshold absorbed power of 500 mW were observed.

The time dependence of the laser output is shown in Fig. 3. The upper trace (a) shows the laser output when the pump beam is turned on for approximately 4 ms. No spiking is seen at this pump level which is 2.9 times threshold. An expanded scale shows relaxation oscillation in Fig. 3(b) at 5 μs/cm.

Tunable output has been demonstrated in a modified nearly concentric cavity. The output mirror [Fig. 1(h)] was replaced by a 10 cm radius mirror, with reflectivity > 98.5 percent in the tuning region, to allow space for insertion of a single element birefringent filter [Fig. 1(g)]. At an absorbed power of 1.5 W, laser output was observed from 728.8 to 809.0 nm. The FWHM was as low as 1.3 nm near the peak of the tuning range, but widened to 2.7 nm away from the peak.

III. Discussion

The fraction of pump photons converted into laser photons, or quantum efficiency, taking into account laser output at the input mirror, is 69 percent. This fraction is directly related to optical losses in the cavity. The loss can be calculated from the slope efficiency η,

$$\eta = \frac{\lambda_p T o}{\lambda_L (T + L)} \tag{1}$$

where λ_p and λ_L are the pump and laser wavelength, respectively, T_o is the output coupler transmission, T is the total transmission of the cavity mirrors, and L is the round trip sample loss. Using the data in Fig. 2, L = 1.4 percent roundtrip or 2.4 percent/cm single pass.

L can also be determined from the relaxation oscillation in Fig. 3(b). The angular frequency of oscillation Ω is related to the loss L by [10]

$$\Omega^2 = \frac{(\rho - 1)L}{\tau\tau_T} \tag{2}$$

where ρ is the ratio of pump power to threshold pump power, τ is the transition lifetime which is 62 μs, and τ_T is the round trip transit time of the cavity. The result is L = 2.6 percent round trip which is roughly comparable to L determined from η.

The excited state Cr^{3+} ion density at threshold can be estimated [4] assuming the radiative quantum efficiency is near 100 percent and a Gaussian pump beam profile. The radiative quantum efficiency of alexandrite is near 100 percent [11]; emerald is expected to be near 100 percent also. The Gaussian pump beam profile leads to a Gaussian distribution of excited Cr^{3+} ions, $n(r)$, where r is the radial distance from the center of the Gaussian profile. The excited state ion density at $r = 0$ is

$$n(0) = \frac{2P_{th}\tau}{h\nu_p \pi \omega_p^2 l} \tag{3}$$

where P_{th} is the threshold absorbed power (500 mW), $h\nu_p$ is the pump beam photon energy, ω_p is the pump beam waist (60 μm), and l is the sample length (2.8 mm). $n(0) = 6.4 \times 10^{18}$ cm^{-3} which corresponds to 5.8 percent of the total Cr^{3+} ion density. At this low level of excitation, excited-state absorption of the pump beam is not significant.

The observed tuning range of the emerald laser is 728.8-809.0 nm which does not cover the entire fluorescence range of emerald (700-850 nm) because of excited state absorption of the laser photons. The single pass gain of emerald [1], which includes the effect of excited state absorption, shows gain to almost 830 nm, but with only weak gain beyond 810 nm. The tuning results observed here are consistent with the single pass gain measurement.

A comparison of these emerald results to previous alexandrite laser results [4] is summarized in Table I. The higher laser quantum efficiency of alexandrite (85 versus 69 percent) is due to the higher optical quality of alexandrite. The loss in alexandrite is 0.35 percent/cm, almost an order of magnitude smaller than in emerald. The losses in emerald are due to optical distortions rather than scattering or absorbing centers. Large losses also were measured in the first emerald laser which was flashlamp pumped [1]. In a CW laser pumped experiment similar to the one reported here with GdScGa-garnet:Cr^{3+} (GSGG:Cr^{3+}) [7] the loss was 6.5 percent/cm. Presently, one advantage of alexandrite as a laser material is its excellent optical quality. Furthermore, the excellent quality of alexandrite is present throughout the sample. The emerald laser output varied markedly as different areas of the sample were selected for laser action. The results reported here are for a relatively favorable section of the crystal. Emerald, unlike a number of other Cr^{3+} vibronic lasers [3], [7], [8], cannot be grown by the Czochralski process. The crystals used here were grown by the hydrothermal process.

-50-

TABLE I
A COMPARISON OF THE EMERALD AND ALEXANDRITE LASERS IN THE SAME CAVITY

	Emerald	Alexandrite
Laser Quantum Efficiency	69%	85%
Loss	2.4%/cm	0.35%/cm
Free Running Wavelength	765 nm	752 nm
Tuning Range	729-809 nm	726-802 nm

The tuning range of emerald and alexandrite are similar presumably because of similar excited state absorption spectra. The excited state absorption in alexandrite has been measured [12] and is responsible for the long wavelength cutoff of the laser output. The minimum in excited state absorption in alexandrite near 750 nm determines the free running alexandrite laser wavelength [3], [12]. In the same 10 cm nearly concentric cavity described above, alexandrite lases at 752 nm under free running conditions. The emerald laser produces 765 nm output; thus, the minimum in excited state absorption is shifted to near 765 nm. This shift in the minimum of excited state absorption is presumably due to the change in crystal field from alexandrite to emerald. The location of the minimum in other materials can be predicted by comparing the crystal field strength to that of alexandrite and emerald. For example, using the energy separation of the ^2E and $^4T_2$ levels in ruby, alexandrite, and emerald to determine the relative crystal field, the location of the minimum in ruby is extrapolated to be at 703 nm which is near the ruby R line (694 nm). This is consistent with the good R laser characteristics of ruby. Previous measurement of excited state absorption in ruby in the pump bands [13] also gives a similar result. Although these data [13] do not extend to the R line, extrapolation indicates that a minimum in excited state absorption is present near the R lines of ruby.

Finally, heating effects in the laser pumped alexandrite and emerald lasers can also be compared. Alexandrite showed little or no heating effects [4] while emerald showed several heating effects described earlier. This difference is due to the fact that emerald has a thermal conductivity which is four times less than that of alexandrite.

ACKNOWLEDGMENT

We thank A. G. Davis for technical assistance and R. C. Morris and H. P. Jenssen for helpful discussions during this work.

REFERENCES

[1] M. L. Shand and J. C. Walling, "A tunable emerald laser," *IEEE J. Quantum Electron.*, vol. QE-18, pp. 1829-1830, Nov. 1982.

[2] M. L. Shand, "The emerald laser," R. C. Powell, Ed., in *Proc. Int. Conf. Lasers '82*. McLean, VA: STS Press, pp. 799-802, Dec. 1982.

[3] J. C. Walling, O. G. Peterson, H. P. Jenssen, R. C. Morris, and E. W. O'Dell, "Tunable alexandrite lasers," *IEEE J. Quantum Electron.*, vol. QE-16, pp. 1302-1315, Dec. 1980.

[4] S. T. Lai and M. L. Shand, "High efficiency CW laser-pumped tunable alexandrite laser," *J. Appl. Phys.*, Oct. 1983.

[5] J. C. Walling, H. P. Jenssen, R. C. Morris, E. W. O'Dell, and O. G. Peterson, "Tunable laser performance in $BeAl_2O_4:Cr^{3+}$," *Opt. Lett.*, vol. 4, pp. 182–183, June 1979; see also C. F. Cline, R. C. Morris, M. Dutoit, and P. J. Harget, "Physical properties of $BeAl_2O_4$ single crystals," *J. Mater. Sci.*, vol. 14, pp. 941–944, 1979; see also M. L. Shand, J. C. Walling, and H. P. Jenssen, "Ground state absorption in the lasing wavelength region of alexandrite: Theory and experiment," *IEEE J. Quantum Electron.*, vol. QE-18, pp. 167–169, Feb. 1982; see also S. Guch, Jr. and C. E. Jones, "Alexandrite laser performance at high temperature," *Opt. Lett.*, vol. 7, pp. 608–610, Dec. 1982.

[6] J. Buchert, A. Katz, and R. R. Alfano, "Laser action in emerald," in *Proc. Int. Conf. Lasers '82*, R. C. Powell, Ed., McLean, VA: STS Press, pp. 791–798, Dec. 1982; see also "Laser action in emerald," *IEEE J. Quantum Electron.*, vol. QE-19, pp. 1477–1478, Oct. 1983.

[7] G. Huber and B. Struve, "Chromium doped crystals for tunable lasers," in *Proc. Int. Conf. Lasers '82*, McLean, VA: STS Press, Dec. 1982; see also B. Struve and G. Huber, "Tunable room-temperature cw laser action in Cr^{3+}:GdScGa-garnet," *Appl. Phys. B*, vol. 30, pp. 117–120, 1983.

[8] H. P. Christensen and H. P. Jenssen, "Broad-band emission from chromium doped germanium garnets," *IEEE J. Quantum Electron.*, vol. QE-18, pp. 1197–1201, Aug. 1982.

[9] P. T. Kenyon, L. Andrews, B. McCollum, and A. Lempicki, "Tunable infrared solid-state laser materials based on Cr^{3+} in low ligand fields," *IEEE J. Quantum Electron.*, vol. QE-18, pp. 1189–1197, Aug. 1982.

[10] P. F. Moulton, A. Mooradian, and T. B. Reed, "Efficient cw optically pumped Ni:MgF laser," *Opt. Lett.*, vol. 3, pp. 164–166, Nov. 1978.

[11] M. L. Shand, "The quantum efficiency of alexandrite," *J. Appl. Phys.*, vol. 54, pp. 2602–2604, May 1983.

[12] M. L. Shand and J. C. Walling, "Excited-state absorption in the lasing wavelength region of alexandrite," *IEEE J. Quantum Electron.*, vol. QE-18, pp. 1152–1155, July 1982.

[13] W. M. Fairbank, Jr., G. K. Klauminzer, and A. L. Schawlow, "Excited-state absorption in ruby, emerald and $MgO:Cr^{3+}$," *Phys. Rev. B*, vol. 11, pp. 60–76, Jan. 1975.

0018-9197/84/0200-0108$01.00

THE EMERALD LASER
Michael L. Shand
Corporate Research and Development
Allied Corporation
P.O. Box 1021R
Morristown, NJ 07960 USA

ABSTRACT

Emerald is a new broadly wavelength-tunable vibronic laser with higher gain than alexandrite. Gain depends on polarization direction and is largest for polarization parallel to the hexagonal axis. The physical properties of beryl are consistent with those of a good solid-state laser host.

INTRODUCTION

Emerald [$Be_3Al_2(SiO_3)_6:Cr^{3+}$] is similar to ruby and alexandrite in electronic structure.[1,2] The lowest energy levels which contribute to the emission spectra of these materials are shown in Fig. 1. The ^2E level gives rise to sharp emission, the R lines. The $^4T_2$ level gives rise to broad emission which terminates in the vibronic bands of the ground electronic state. The excited states are in thermodynamic equiblibrium[3] so that the energy gap, ΔE, between the ^2E level and the $^4T_2$ level determines the relative population

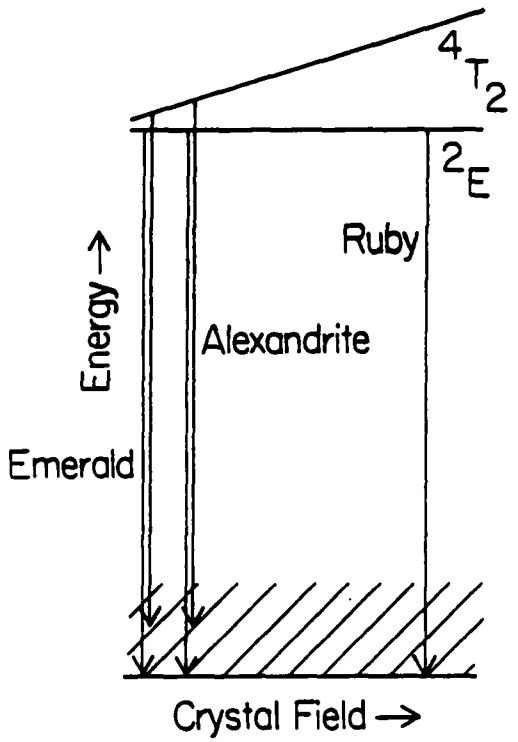

Figure 1 Energy levels of Cr^{3+}.

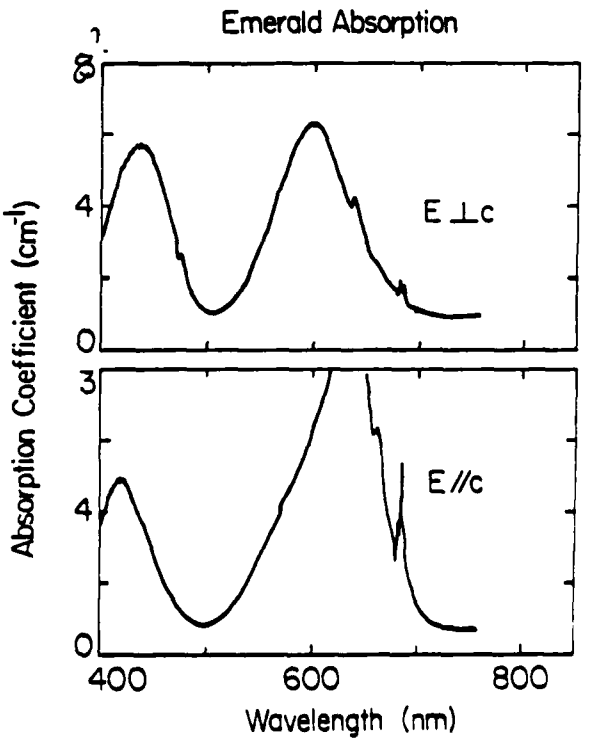

Figure 2 Absorption in emerald.

of the $^4T_2$ level and thus the strength of the vibronic emission. ΔE in emerald is approximately 400 cm^{-1} while ΔE in alexandrite is approximately 800 cm^{-1}. ΔE in ruby is about 2300 cm^{-1} and no vibronic emission is observed at room temperature. Alexandrite has already been shown to be a good laser material,[1,4] so that frequent comparison of emerald to alexandrite will be made in this paper.

PROPERTIES OF BERYL

Some of the physical properties of beryl [$Be_3Al_2(SiO_3)_6$] are shown in Table I. Beryl is not quite as hard as chrysoberyl (undoped alexandrite) but is hard enough to be handled conveniently. The linear thermal expansion of beryl is one-fifth that of chrysoberyl, which indicates a very good laser host. On the other hand, the thermal conductivity of beryl is one quarter that of chrysoberyl. Nevertheless, the thermal conductivity is only a little less than that of yttrium aluminum garnet (YAG). Taken together, the physical properties of beryl are consistent with those of a good solid-state laser host.

TABLE I Physical properties of beryl.[5]

Density	2.66 gm/cm^3
Hardness (Mohs Scale)	7.8
Linear Thermal Expansion	
//c	1.35 x 10^{-6} per °C
⊥c	1.00 x 10^{-6} per °C
Thermal Conductivity (40°C)	
//c	5.50 x 10^{-2} W/cm -K

EMERALD SPECTROSCOPY

The absorption coefficient of typical emerald (~1.8 at. % Cr^{3+}) is shown in Fig. 2. The strong Cr^{3+} absorption bands in the visible show that emerald can be readily pumped by flashlamps or laser excitation. The room temperature lifetime, τ, of 50 μs also is reasonably convenient for flashlamp excitation. The two spectra shown in the figure correspond to absorption for light polarized parallel or perpendicular to the unique axis (c-axis) in emerald which has hexagonal structure.

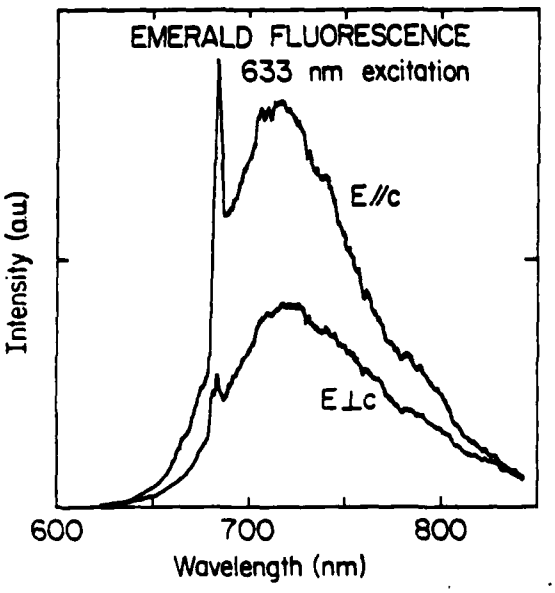

Figure 3 Emerald fluorescence.

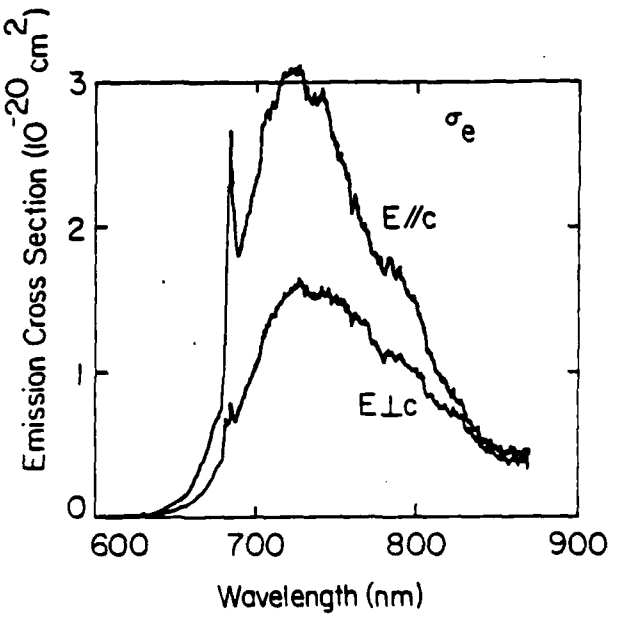

Figure 4 Emerald emission cross section.

The fluorescence spectra of emerald for the two independent polarization directions are shown in Fig. 3. The broadband emission is evident. The R line appears weaker than in alexandrite as expected. However, the peak intensity of the R line emission may not be accurate because of (1) limitation of resolution in the spectrometer used in the study and (2) reabsorption of R line fluorescence as it traverses the sample. Efforts to minimize the latter effect were taken such as illuminating the sample near the front surface; nevertheless, some reabsorption is unavoidable. Low Cr^{3+} concentration samples will be obtained to determine an accurate fluorescence spectrum. Note that the emission from E//C is twice that of E⊥c.

The emission cross section $\sigma_e(\lambda)$ can be determined from the fluorescence spectra $I(\lambda)$ using the formula:

$$\sigma_e(\lambda) = \frac{3\lambda^5 I(\lambda)}{(\Sigma\int\lambda I(\lambda)d\lambda)\tau 8\pi n^2 c} \quad (1)$$

where the summation is over three orthagonal polarization directions, the integral is over the entire emission band, n is the index of refraction of emerald and c is the speed of light. The resulting $\sigma_e(\lambda)$ is shown in Fig. 4. For the reasons cited earlier, σ_e(R lines) may be somewhat smaller than in reality. Buchert et al.[6] have observed laser emission on the R line indicating that the R line must have larger σ_e than the vibronic band. σ_e//c is roughly twice σ_e⊥c. The breadth of $\sigma_e(\lambda)$ indicates lasing could occur out to 850 nm or beyond. The peak σ_e of alexandrite is only 0.7 x 10^{-20}cm^2 (1/5 that of emerald) but shows similar breadth; however, alexandrite only lases out to ~805 nm at room temperature because of excited-state absorption. The effect of the excited-state absorption cross section $\sigma_{2a}(\lambda)$ on gain can be seen by measuring the single pass gain.

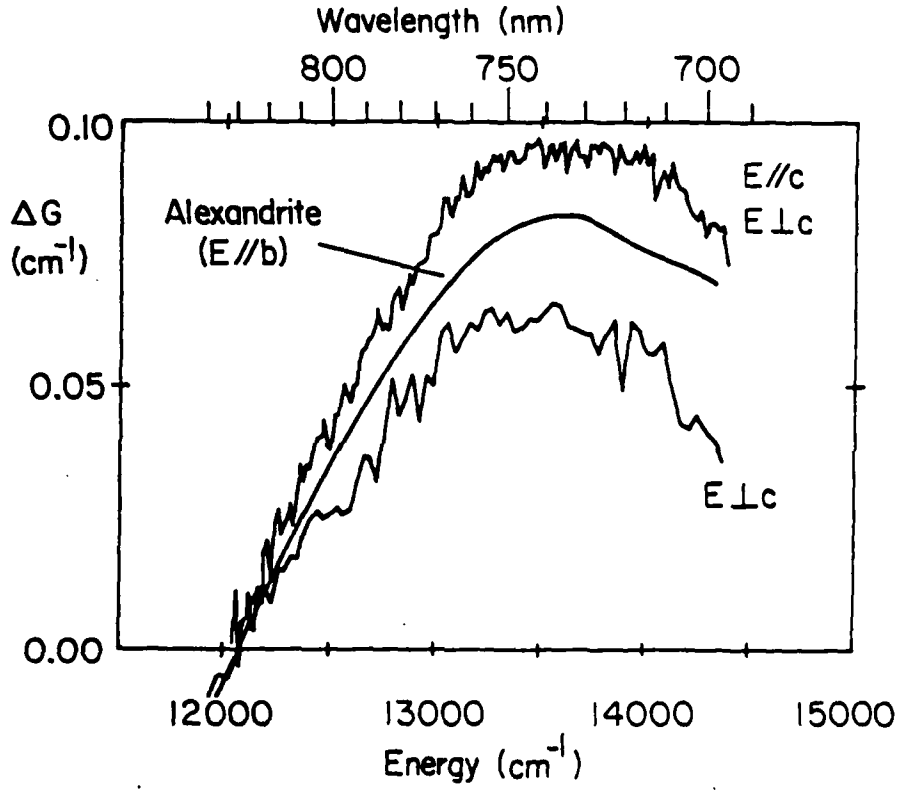

Figure 5 Single pass gain in emerald and alexandrite.

The single pass gain (SPG) of emerald has been measured previously[7] and is shown in Fig. 5. The SPG was measured in a rod with the c-axis at ~45° to the rod axis. The two polarization directions available are therefore E⊥c and E with equal components of ⊥c and //c. A SPG result for a similar alexandrite rod is also shown in the figure. The estimated gain for emerald, E//c is approximately twice that of alexandrite. The gain becomes zero at low energy at approximately 825 nm. At lower energies, $\sigma_{2a} > \sigma_e$ and no lasing is possible. If the fraction of excited Cr^{3+} ions (p^+) during the SPG measurement were known, $\sigma_{2a}(\lambda)$ could be determined. p^+ has not been measured; however, p^+ has been measured for alexandrite in the same cavity and leads to p^+ in emerald of 10% to 20%. Using these estimates the peak value of σ_{2a} is (0.3 - 1.7) x 10^{-20} cm^2 for E//c and (0.2 - 0.8) x 10^{-20} cm^2 for E⊥c. Thus σ_{2a} in emerald appears to be larger than in alexandrite and may possibly be significantly larger than in alexandrite.

Emerald Laser

The first emerald laser has been described previously.[7] The laser oscillator had a 19 x 4 mm diameter rod, again with the c axis at approximately 45° to the rod axis. The rod was mounted in the same water-cooled ceramic flashlamp cavity used in the SPG measurements. The optical cavity was formed with a high reflector and a 95 percent reflectivity output coupler. Both mirrors were concave with a 4 m focal length. The laser emitted 6.8 mJ at 757.4 nm. With output mirrors having different reflectivity spectra, the laser operated at wavelengths from 751.1 to 759.2 nm. The laser had large losses ($\approx 0.11\ cm^{-1}$), presumably due to beam breakup which is caused by planes in the crystal having slightly different indexes of refraction. Each of these growth planes, along which the index of refraction is constant, is parallel to the others and perpendicular to the direction of crystal growth. Beam breakup is caused by reflection from these planes, and can be observed by passing a probe beam through the crystal. The losses can be minimized by directing the probe beam parallel to these planes and the laser rod described above was cut with the rod axis approximately parallel to these planes. However, the losses are only minimized and are not eliminated.

The beam breakup can be avoided completely by propagating the beam at large angles to these planes such as in a slab laser.[8] In a slab laser geometry the laser beam propagates through the emerald crystal in a zig-zag fashion with a propagation direction at a large enough angle relative to the planes of varying index such that no beam breakup is observed. A slab laser is also particularly useful when the active medium is pumped hard which is the case for low gain materials such as the vibronic laser crystals.

Conclusions

Emerald is a broadly wavelength-tunable vibronic laser with higher gain than alexandrite. Gain depends on polarization direction and is largest for polarization parallel to the hexagonal axis. The physical properties of beryl are consistent with those of a good solid-state laser host. The slab geometry laser is particularly suitable for emerald.

Acknowledgements

H.P. Jenssen and R.C. Morris have made helpful comments on the manuscript and A.G. Davis has contributed technical assistance to this project.

References

[1]J.C. Walling, O.G. Peterson, H.P. Jenssen, R.C. Morris and E.W. O'Dell, "Tunable Alexandrite Lasers," IEEE J. Quantum Electron, QE-16, 1302, 1980.

[2]P. Kisliuk and C.A Moore, "Radiation from the $^4T_2$ State of Cr^{3+} in Ruby and Emerald," Phys. Rev. 160, 307, 1967.

[3]M.L. Shand, J.C. Walling and H.P. Jenssen "Ground State Absorption in the Lasing Wavelength Region of Alexandrite: Theory and Experiement," IEEE J. Quantum Electron. QE-18, 167, 1982.

[4]D.R. Siebert, J.J. Barrett, J.C. Walling, M.G. Cullison and G.L. Schuh, "High Peak Power Performance of Alexandrite," Conference on Lasers and Electro-Optics, Technical Digest, April, 1982, Optical Society of America, 1982, p. 160.

[5]Handbook of Chemistry and Physics, 42nd Edition, Chemical Rubber Publishing Co., Cleveland, 1961.

[6]J. Buchert, A. Katz and R.R. Alfano, "Laser Action in Emerald," Proceedings, this conference, Lasers '82, Dec. 1982, New Orleans, Society for Optical and Quantum Electronics, McLean, VA.

[7]M.L. Shand and J.C. Walling, "A Tunable Emerald Laser," IEEE J. Quantum Electron. Letters, QE-18, 1829, 1982.

[8]J.M. Eggleston, T.J. Kane and R.L. Byer, "Slab Geometry Solid State Lasers," Conference on Lasers and Electro-Optics, Technical Digest, April, 1982, Optical Society of America, 1982, p. 112.

END

11-86

DTIC